Research Article

Gain and radiation pattern enhancement using ANN-based reflector antenna for full 5G Sub-6GHz applications

Shabnam Ara[1*] and Prasanthi Kumari Nunna[2]
Research Scholar, School of Engineering & Technology, University of Petroleum & Energy Studies, Dehradun (Uttarakhand), India[1]
Associate Professor, School of Engineering & Technology, University of Petroleum & Energy Studies, Dehradun (Uttarakhand), India[2]

Abstract
The development, analysis, fabrication, and measurements of an inset-feed frequency selective surface (FSS) monopole rectangular patch antenna based on the Fabry-Perot cavity (FPC) principle were discussed in this paper. The proposed antenna is fabricated on two pieces of flame retardant-4(FR4) substrate (FSS reflector) and RT Duroid 5880 substrate (main radiating patch) of equal size 49mm×49mm×1.6mm. The use of FR4 controls the cost of the antenna while the RT Durid maintains low losses and supports improvement in gain and radiation characteristics. The FPC principle is utilized to enhance antenna gain and directional radiation characteristics. The distance between the substrate and FSS layer is evaluated by developing a relationship using a machine learning artificial neural network (ANN) model-based method by speculating the output through iterations and it is validated by the high-frequency structure simulator (HFSS) optimization process. Equally spaced 15 dipole strips FSS layer is used as reflector surface which yields enhanced gain from 4.41dBi to 8.99dBi (∽4.58dBi improvement), unidirectional radiation patterns, and improved front-to-back-ratio (FBR) from 1.7dB to 17.5dB in the E-plane at the design frequency 5.5GHz. The antenna achieves a -10dB bandwidth from 1.12GHz to 8.64GHz (7.52GHz). The measured results are in close agreement with the simulated results. At the end, an electrical equivalent resistor, inductor, and capacitor (RLC) circuit of the proposed antenna has been generated from the antenna reflection coefficient. The reflection coefficient of the RLC equivalent circuit of the proposed antenna is validated using advanced design system (ADS) software. Since the antenna has ultra-wideband (UWB) performance, therefore it is most suitable for wireless 3G/4G/5G and Sub-6GHz lower frequency range (FR1), satellite, and RADAR communications.

Keywords
Artificial neural network (ANN), Dipoles, Frequency selective surface (FSS), Gain enhancement, Wideband (WB).

1. Introduction
The antenna is a vital component of radio engineering. Every transmitter and receiver contains an antenna and plays a key role between radio waves traveling over space and electric currents flowing via metal conductors. The first microstrip patch antenna was developed in 1953. The advancement of wireless communication technology has made research work and the design of microstrip patch antenna structures more appealing. Due to its low profile, low cost, lightweight, and ease of fabrication, microstrip patch antennas have innovative suggestively in research as compared to conventional antennas.

The performance of the antenna is largely dependent upon the substrate's physical characteristics [1, 2]. The main patch, substrate, and ground plane are arranged in a sandwich-like pattern on a rectangular microstrip patch antenna. The antenna is a key element in the development of microstrip to rectangular waveguide transition, microstrip to substrate integrated waveguide (SIW) transitions, transmitter-receivers front end, microwave components, monolithic microwave integrated circuits (MMIC) and devices, etc [3, 4]. Antennas are used to launch radio frequency energy into the waveguides. Nowadays different types of planar antennas using the latest technologies like fractal, metamaterials, and switchable frequency reconfigurable have been developed and further

---

*Author for correspondence

research is going on. The microstrip antennas have now become the most popular and most widely used by wireless, satellite, and radar applications [5–7]. In the present scenario, with the development of mobile technologies like the 3rd generation/4th generation/5th generation/6th generation (3G/4G/5G/5G), the demand for 5G/6G antenna is increasing [8]. Therefore, the demand for antennas that will cover 5G Sub-6GHz FR1 (< 7425MHz) bands, especially n77, n78, and n79 is now necessarily important [9]. The above-designed antennas are complex in geometry because of the use of metamaterials and fractal technologies, thus their fabrication is difficult, and these are suitable for multi-band and wide-band applications. These antennas have bi-directional radiation characteristics and suffer from limited gain. Therefore, it is necessary to design a simple structure, the easily fabricable antenna that could cover all the 5G frequency bands or even all-important 5G bands with ultra-wide band (UWB) performance, and have high gain with directional radiation characteristics using the latest technologies like frequency selective surface (FSS), superstrate, artificial magnetic conductors (AMC), reflectors, etc [10–12]. The FSS reflector is used as a reflector to enhance the gain of the planar antennas and also improve the directional radiation characteristics [13, 14]. FSS is a periodic structure of unit cells that consists of metallic patches or space components with good transmission or reflection properties [15].

The following are the main objectives of the proposed work;

(i)The primary objective of the present study is to design a simple rectangular patch antenna to cover the full range of Sub-6GHz applications with main concern on n77(3300-4200MHz), n78(3300-3800MHz), and n79(4400-5000MHz) bands.

(ii) The second objective of this research is to enhance the antenna gain and directional radiation characteristics by arranging the FSS layer as a reflector at a suitable distance beneath the ground of the main radiator using two separate substrates for each.

(iii) The third objective of this work is to develop an electrical equivalent resistor R, inductor L, and capacitor C (RLC) model and validate the same using the advanced design system (ADS).

(iv) To use the a ANNs optimization method to determine the optimum distance of the reflector FSS layer from the main patch radiator.

The article is organized in such a way that section 2 describes the detailed literature review of related

work. Section 3 explains the proposed antenna design development method, the machine learning methodology used for the substrate separation evaluation, and antenna parametric optimization. The subsequent sections 4 and section 5 present the analysis of the simulated and measured results and their discussions along with literature-similar antenna comparisons. Finally, the work is concluded with future suggestions in section 6.

2. Literature review

Nakmouche et al., have presented an enhanced gain FSS superstrate reflector surface-based monopole antenna using machine learning. The authors arranged a superstrate FSS layer above 6.0 mm distance from the main radiator which enhance the gain from 3.12dBi to 8.89dBi [16]. Belen has developed an FSS antenna that results in the enhancement of gain 7.15dBi for the industrial scientific and medical (ISM) radio band [17]. Sarkhel and Bhadra, have explained a gain enhancement method for slotted antenna by the use of an electric metasurface superstrate. This enhances the broadside gain and efficiency by 10.86dBi and 20.35% respectively [18]. Fernandes et al., have proposed an FSS reflector dual-band antenna. The FSS layer one unit cell consists of a concentric quad square ring pair for the ISM band. This led to a gain enhancement of 7.54 dBi and 6.8 dBi at dual frequencies 2.4 GHz and 5.8 GHz even though it has a larger FSS size than the main radiator substrate and a less front-to-back ratio (FBR) [19]. Tilak et al., have demonstrated a heart-shaped monopole antenna using an AMC for gain and radiation properties improvement. The antenna with the use of a 3 × 3 AMC structure at $\lambda_0/4$ distance increases the gain from 1.8 dBi and 2.21 dBi to 5.86 dBi and 7.20dBi at the 3.5GHz Wi-MAX band and 5.8 GHz wireless local area network (WLAN) applications [20]. Gharsallah et al., have discussed a dielectric resonator antenna (DRA) using a split ring resonator (SRR) superstrate surface for the enhancement of gain to 11.15dBi [21]. Ram and, Kumar, have proposed a planar-slotted ground UWB (3.2GHz to 12GHz) antenna with an FSS reflector. Both the antenna radiator and FSS layer are fabricated on the two same type of substrate. The antenna attains an enhanced gain of 3dBi to 4dBi over the full band with reduced cross-polarization [22]. Bhattacharya et al., have developed an ultra-thin FSS surface for gain enhancement using a low-loss Rogers RT Duroid 5880substrate. This double-layered FSS is applied on the dielectric resonator hybrid slotted antenna. It results in a gain enrichment of 7.8dBi [23]. Hussain et al., have proposed a

coplanar waveguide (CPW) fed spades-shaped antenna using a 5×5 square circular FSS for bandwidth and gain enhancement and UWB applications. This FSS antenna enhances the peak gain from 6.5dBi to 10.5dBi [24]. Ranga et al., have developed a multi-octave FSS reflector for UWB antenna to maintain the antenna gain constant 7.5dBi over the entire band from 3GHz to 7GHz [25]. Devarapalli et al., have proposed an FSS-based dual complementary split ring resonator (CSRR) loaded W-shaped patch antenna. This FSS metamaterial-loaded antenna has provided an improved gain from 5.9dBi to 7.1dBi with triple-tuned resonances at frequencies of 4.2, 6.2, and 8.0 GHz. The antenna structure is low-cost and complex with CSRR loading [26]. Tewary et al., have developed an FSS-based wideband (WB) S-shaped slotted ground microstrip patch antenna for 5G communication, RADAR, satellite services, and wireless communications. That achieves a gain of 3.9 dBi at 19.0 GHz without applying FSS. Introduced FSS in the antenna enhances gain, BW, and directivity. The antenna with FSS achieves a maximum gain of 9.4 dBi at 22.1 GHz and a widened -10dB FBW of 111%. The antenna is low profile, low-cost as fabricated on flame redundant-4 (FR4) substrate, and its FSS layer is larger as compared to the main radiating patch antenna. The used substrate of this antenna is not valid in the proposed frequency sweep because it has undergone nonlinearity of permittivity and dispersion losses at above 6.0 GHz. The 15.0mm separation between FSS and the radiating patch increases the overall volume of the antenna [27]. Tewary et al., have presented a super-wideband (SWB) monopole antenna for long-distance communication. The suggested SWB antenna has a 4.80 dBi realized gain. The FSS acts as a partial reflector surface and is coupled with the proposed antenna to enhance the maximum gain. The introduced FSS (physical volume of 56 mm × 56 mm × 26.2 mm) achieves an improved antenna realized gain of 9.3 dBi. The proposed antenna with FSS not only enhances gain but also enhances the bandwidth. The size of FSS is still large and its distance from the main patch is 26.2mm. Therefore, its overall volume also increases [28]. Further, Tewary et al., have demonstrated an N-shaped antenna with FSS. This antenna has a significant -10 dB FBW of 138%, resonance at 14.55 GHz, and a peak gain of 4.45 dBi at 9.5 GHz. The antenna attains a maximum gain enhancement of 7.5 dBi at 3.5 GHz and a peak gain of 9.1 dBi at 9.3 GHz [29]. Prasad et al., have suggested a staircase-shaped printed monopole antenna for wireless applications loaded with a novel FSS structure. That FSS leads to

improving the performance parameters of the developed antenna. The dual bands antenna (2.18-2.83GHz and 4.42 to 5.58 GHz) achieves a fractional impedance bandwidth of 25.94% and 23.2% [30]. Renit and Raj, have fabricated a wearable (flexible denim substrate) dual-band FSS antenna for 5G and Wi-Fi applications. The FSS layer is used to improve the gain of the antenna from 2.6dBi to 7.78dBi and from 3.8dBi to 6.02dBi at 3.5GHz and 5.8GHz respectively. The size of the FSS is greater than the antenna radiator which increases the size and volume complexity [31]. Lanka and Chalasani have designed an M-shaped conformal antenna with FSS support for gain enhancement. The FSS located beneath the antenna and serves as a reflector. This consequently, adds an extra 22% gain, and an increase of 12% in antenna efficiency [32]. The FSS layer is mounted over the main radiator (superstrate) with a predetermined air gap to boost the antenna performance. The FSS (as a bandpass filter) rejects the unused frequencies and passes only the necessary ones. Perhaps, the gain and bandwidth of the antenna increase. However, in the second design, the overall antenna's performance will be improved with the use of the array structure [33]. Danuor et al., have designed a rectangular patch with several matching stubs surrounding it to increase the antenna's impedance bandwidth for the L-band and S-bands at 1.6–2.1 GHz and 2.4–2.85 GHz, respectively. The antenna's rear side was printed with three unit cells that behave as the FSS layer. Moreover, the antenna achieved radiation efficiencies of 89.7% and 94.2% at 2.5 GHz and 1.7 GHz, respectively. The measured average gain of the suggested antenna for the L-band and S-band is 5.2 dBi and 6.1 dBi, respectively [34]. Tariq et al., have proposed an FSS sheet to enhance the antenna's performance. A sheet of FSS was positioned beneath the antenna to increase antenna gain and the antenna's backward reflection. It enhances the antenna's gain from 4.5 dBi to 9.5 dBi [35]. Hossain et al. have presented a slotted circular patch antenna that enhances the antenna's gain and radiation efficiency. The defective ground structure (DGS) was used to increase its bandwidth. The antenna is small, with dimensions 12 × 12 mm square. This antenna achieves a wide bandwidth of 19.73 GHz and a maximum efficiency of 91%. The antenna's back end at a 5.0 mm air gap uses an FSS with an L-shaped unit cell to boost gain. It achieves a maximum gain of 8.24 dBi [36]. Ara and Nunna have proposed a rectangular patch antenna with FSS. The introduced FSS enhances the gain of 7.76dBi (an improvement of 4.91dBi) and an increased -10dB FBW (3.90GHz to 6.43GHz), FSS also converts the

bidirectional radiation pattern into a unidirectional one and greatly increasing the FBR. Additionally, the antenna's radiation efficiency is 94.68% at the resonance frequency of 5.8GHz without the FSS reflecting surface and raised to 97.88% with the FSS reflecting surface [37].

From the available literature references 36 and 37, it has been deduced that the FSS layer as reflector below the antenna radiator supports enhancement in the antenna gain while the monopole partial/reduced/DGS supports to improve the antenna -10dB FBW. It is clear from the literature references 6, 33, and 36 that most of the research consists of the matrix of the unit cells and the antenna array of elements as in the FSS layer. Most of the literature references 17, 26, and 36 consist of FSS size greater than the radiator size which results in an increase in volume and extra need for space. Above 6GHz frequencies, researchers used an FR4 substrate for the main antenna radiating patch design. According to Reference 1's information, dispersion losses, variations in effective permittivity, and nonlinearity in the loss tangent cause FR4 to perform poorly beyond 6 GHz. All the available designs in the literature using FSS have complex geometries of radiator and reflector and use the same substrate for the fabrication of the reflector and the radiator design. Most of the existing antennas in literature are multi-band in nature with narrow bandwidths and lower gain values. Furthermore, they have a limited number of applications. The above research gaps motivate us to work on the following areas collectively.

The following are the main challenges of the present research;
-Proper selection of substrate for radiator design to limit the losses as per the frequency sweeps.
-Reduces the complexity of the FSS structure with enhancement in the antenna gain and bandwidth.
-Reduce the overall volume of the antenna by reducing the area of the FSS layer not more than the radiator substrate and reducing the air gap between the radiator and FSS reflector substrates.

In this paper, two different substrates are used for the fabrication of the main antenna patch radiator (RT Duroid 5880) and FSS reflector (FR4) design. The reflector FSS layer enhances the antenna gain and also excellently improves the directional radiation characteristics for RADAR and satellite applications. Antenna achieves an UWB bandwidth of 7.52GHz with a high gain value of 8.99dBi which is the novel

achievement of this work since it is a great challenge to get one parameter (gain/bandwidth) enhanced value that opposes the other parameter (bandwidth/gain), since the gain and bandwidth product is constant. The simple structure of the radiator and reflector surfaces makes the antenna fabrication easier. The area of the FSS layer is reduced (equal to the substrate of the radiating patch) and the air gap between the radiator and the FSS reflector substrate decreases. These two effect jointly reduce the overall volume of the antenna. A further contribution of this work is that the radiator and reflectors are fabricated on separate substrates this makes the antenna low-loss and the antenna can operate up to a higher frequency range. Previously designed antennas were fabricated on lossy low-cost FR4 substrate up to higher frequency ranges even though FR4 is not a suitable substrate for fabrication above 6GHz or 8GHz. Another advantage of this research is that it achieves a UWB bandwidth from 1.12GHz-8.64GHz with excellent gain performance and a reflection coefficient below -10dB. This UWB covers all the Sub-6GHz applications along with some RADAR and satellite applications. It is suitable candidate for Sub 6GHz communications like n46 (5150-5925MHz), n47 (5855-5925MHz), n77 (3900-4200MHz), n78(3300-3800MHz), n79 (4400-5000MHz), n96/n102 (5925-6425MHz) etc bands. A simple FSS layer design (consisting of 15 dipole strips) is proposed in this manuscript that eliminates the need for complex designed metamaterial/metasurfaces.

3. Methods
3.1 Fabry-Perot cavity principle
The proposed antenna utilizes the Fabry-Perot Cavity (FPC) principle for the gain enhancement of the single layer antenna. Fabry-Perot Cavity Antennas (FPCAs) are a highly directive planar antenna that offers a promising alternative to standard planar microstrip patch arrays or waveguide slot array antennas. These antennas have the advantage of low fabrication complexity, high radiation efficiency, and good radiation pattern performance, particularly at mm wave frequencies. These advantages, in conjunction with a renewed interest in periodic surfaces and meta-surfaces, led to a reinvigoration of international research on this antenna type. This work reports recent advances on the design and implementation of FPCAs at mm-wave bands. The main concept of FPCAs, their operating principles and analysis approaches are briefly introduced. Many antenna designs were available in literature based on the FPC principle. In this principle, multiple layers

had been used for multi-reflections of the waves and in-phase waves become additive and transmitted while out-of-phase waves cancel out each other. A Fabry-Perot Cavity Antenna (FPCA) consists of a feed antenna, a partially reflective superstrate, and a partial/full metal ground surface [38]. The radiated electromagnetic waves from the driven feed undergo multiple reflections within the cavity. The gap between the metal ground and superstrate is close to the guided wavelength [39, 40]. In FPCAs, partially reflective superstrates are used to achieve a high gain [41]. The relative gain and resonant cavity height of an FPCA can be calculated as,The proposed antenna uses the Fabry-Perot Cavity (FPC) principle to enhance the single-layer antenna's gain. There is a promising alternative to standard planar microstrip patch arrays or waveguide slot array antennas called FPCAs. FPCAs are highly directive planar antennas. These antennas have the advantages of low fabrication complexity, high radiation efficiency, and good radiation pattern performance, particularly at mm wave frequencies. These advantages, in conjunction with a renewed interest in periodic surfaces and meta-surfaces, led to a reinvigoration of international research on this antenna type. This study reports recent advances in the design and implementation of FPCAs in mm-wave bands. The work briefly introduces the main concept of FPAs, their operating principles, and their analysis approaches. The literature contains numerous antenna designs based on the FPC principle. This principle employs multiple layers to multi-reflect the waves, resulting in the additive transmission of in-phase waves and the cancellation of out-of-phase waves. A FPCAs consists of a feed antenna, a partially reflective substrate, and a partial or full metal ground surface [38]. The driven feed's radiated electromagnetic waves undergo multiple reflections within the cavity. The gap between the metal ground and superstrate is close to the guided wavelength [40, 41]. The antenna uses partially reflective superstrates in FPCAs to achieve a high gain [41]. The relative gain and resonant cavity height of an FPCA can be calculated as follows (Equation 1, Equation 2 and Equation 3).

$$G_{Relative} = 10Log(\frac{1+S_{11}}{1-S_{11}}) \tag{1}$$

$$G = \frac{\lambda_0}{4\pi}(\varphi_R + \varphi_G + 2N\pi) \tag{2}$$

The bandwidth of the FPCA is given by,

$$Bandwidth = \frac{\lambda_0}{2\pi G}(\frac{1-S_{11}}{\sqrt{S_{11}}}) \tag{3}$$

Where,

S_{11}=Reflection coefficient of the superstrate,
$G_{Relative}$ = Relative gain,
λ_0= Working wavelength,
G = Cavity height,
φ_R= Reflection phases of the superstrate
φ_G= Reflection phases of the ground

3.2 ANN design approach block diagram and antenna design flow chart

ANN design approach block diagram to obtain the height/FSS reflector seperation from the main antenna is Shown in *Figure 1* (left side) and the antenna design flow chart is illustrated in the *Figure 1* (right side).

The following steps are followed to obtain the proposed antenna structure:

Step 1: Collection of data samples –The resonance frequencies (f_r), reflection coefficients (S_{11}), Voltage Standing Wave Ratio (VSWR), and antenna gain (G) are recorded as data samples. A total 6137 data samples have been collected from the previous simulated results of the FSS antennas.

Step 2: The 70% of data sets are used for training, 15% data sets for validation, and 15% of data sets are used for the testing purposes.

Step 3: The Levenberg-Marquardt learning algorithm was employed. The authors continue this training process until it reaches saturation.

Step 4: Using the ANN algorithm, calculate the predicted height of the FSS reflector under the antenna.

Step 5: The substrate selection is based on the design frequency and selected antenna applications. The FR4 is selected for the FSS reflector design, and the RT Duroid 5880 is chosen for the main antenna design so that the dielectric losses are less and excellent gain and radiation performances come.

Step 6: Design of FSS reflector and main antenna using electromagnetic Simulator.

Step 7: Simulate and optimize the design until the best reflection coefficients, antenna gain, and radiation efficiency are obtained.

Step 8: Once favourable results are obtained fabricate the antenna and then send the antenna in laboratory for testing purpose.

Step 9: Compare the simulated and measured results for antenna validiations.

Step 10: Analyis the other secondary parameters from the primary obtained results.
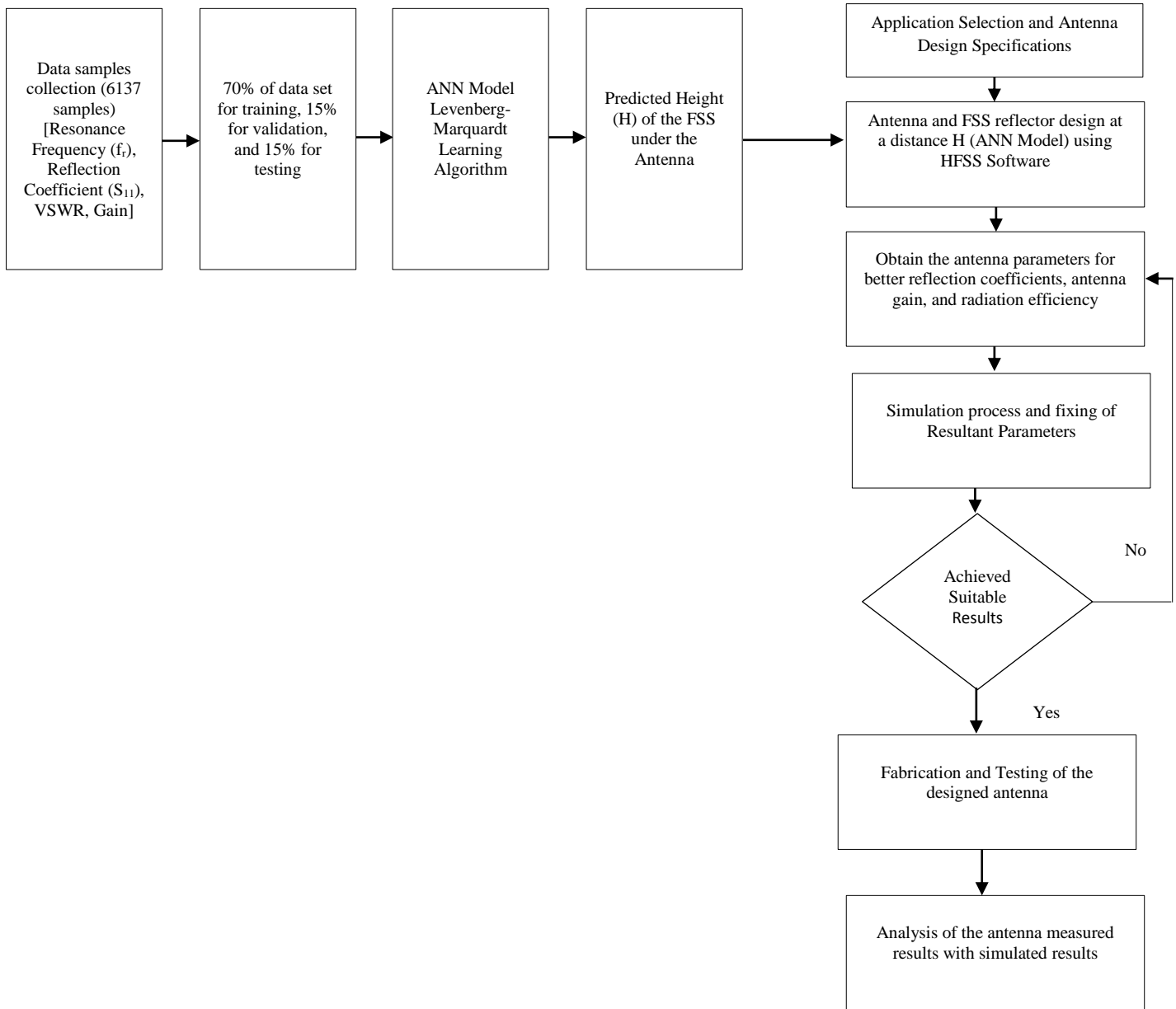
Figure 1 Block diagram of the ANN design approach and flow chart of the antenna design

3.3 Design development

The rectangular patch antenna is designed at a frequency of 5.5 GHz using primarily design equations [42, 43]. The antenna radiator is developed on a low-loss RT Duroid 5880 with a relative permittivity of 2.2 and a height of 1.588mm. However, the FSS is developed and designed on an FR4 substrate with a relative permittivity of 4.4 and a height of 1.588mm. The separation between the two substrates is kept at 8mm, which was evaluated using an ANN model. The FSS is applied beneath the ground of the main radiator. The patch length and width are evaluated at 21.56mm and 17.45 mm, respectively, and finally optimized to 21.55mm and 17.5mm. Initially, the RT Duroid 5880 substrate length was evaluated at 31.088mm and 42.158mm and finally optimized to 49mm on each side. The same-size reflector FSS FR4 substrate was chosen. Therefore, the final antenna size becomes 49mm×49mm×8mm (1.368,λg.×1.368,λg.×0.22,λg.) at the design frequency of 5.5 GHz. An array of 15 equally spaced (1.0mm) dipole strips of length 49mm and width 2mm is used as an FSS reflector and etched on a lossy FR4 substrate. This improves the

patch antenna's gain and radiation characteristics in one direction. The following Equations 4 to 8 are secondary derived formulas that are also used for the evaluation of antenna other dimensional parameters;

Inset feed length, $L_i = L_F - L_{cut}$ (4)

Inset feed Gap/width, $W_i = \frac{W_{cut} - W_F}{2}$ (5)

Length of dipole, $L_{diopole} = L_{sub}$ (6)

Width of ground, $W_{Gnd} = W_{sub}$ (7)

Length of the ground, $L_{Gnd} = \frac{\lambda_g}{4}$ (8)

The substrate Rogers RT Duroid 5880 was chosen for patch design at a frequency of 5.5GHz. According to reference 1, the main rationale behind the choosing substrate is its low loss and stable behavior of permittivity after 6GHz. The results of radiations and reflection coefficients of the proposed antenna have been studied for a frequency sweep from 1GHz to 9 GHz. The low-cost FR4 substrate shows nonlinear behavior of permittivity and loss tangent as frequencies go higher than 6 GHz. The reflector FSS is designed on a low-cost FR4 substrate since it is used only for the reflecting layer. Only the copper conductor will play a role in the reflection of the excitation signal. The dimensions of the radiating patch are evaluated at design frequencies. The antenna dimensions of the substrate are kept equal to $(L_{sub} = L_f + L_p + 3h) \times (W_{sub} = 3h + W_p + 3h)$. The spacing between the radiator and FSS substrate is kept less than or equal to the quarter-guided wavelength $(H = \frac{\lambda_g}{4})$ so that the reflected signal will add up to the radiated signal and improve the directional properties and gain.

Figure 2(a) displays the inset-feed rectangular patch radiator, *Figure 2(b)* displays the antenna's ground structure, and *Figure 2(c)* represents the FSS reflector. *Figure 2(d)* showcases the geometry of the proposed antenna design and its all-dimensional representation. *Table 1* lists the evaluated values of the proposed antenna dimensions and compares them with the optimized simulated dimensions in the other column.

(a)   (b)   (c)

(c)
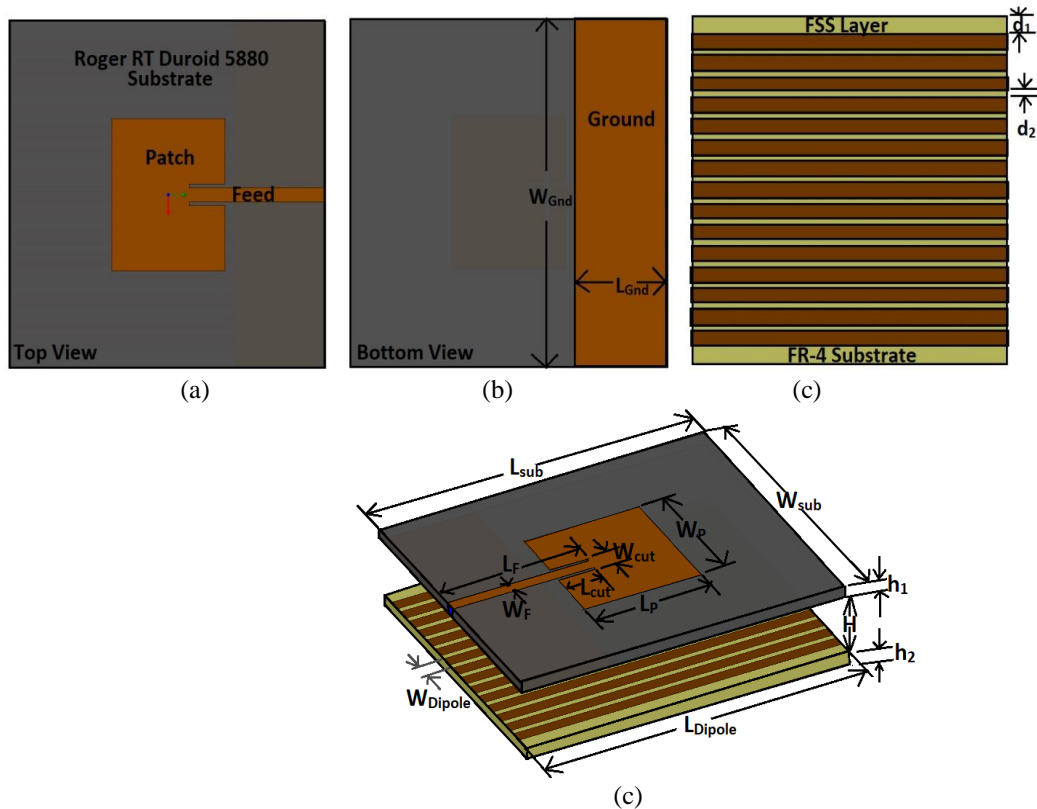
Figure 2 Proposed FSS Antenna (a) Top View, (b) Bottom View, (c) FSS layer, and (d) Dimensional View

Table 1 Proposed antenna design dimensions

Parameter name	Symbolic representation	Evaluated value (in mm)	Simulated or optimized value (in mm)
FR4 and RT Duroid 5880 Substrates width	$W_{sub}= 3h+W_P+3h$	31.088	49.0
FR4 and RT Duroid 5880 Substrates length	$L_{sub}=L_f+L_P+3h$	42.158	49.0
Patch width	W_P	21.56	21.55
Patch length	L_P	17.455	17.5
Microstrip Feed width	W_F	4.893	2.0
Microstrip Feed Length	$L_F=\frac{\lambda_g}{2}$	19.94	21.25
Inset-Cut width	$W_{cut}= W_F+1mm$	0	3.0
Inset-Cut length	L_{cut}	0	5.5
Ground width	$W_{Gnd}= W_{sub}$	31.088	49.0
Ground length	$L_{Gnd}=\frac{\lambda_g}{4}$	9.97	14.25
Height of RT Duroid 5880	h_1	1.588	1.588
Height of FR-4	h_2	1.588	1.6
The gap between two substrates	$H=\frac{\lambda_g}{4}$	9.97	8.0
Width of dipole	$W_{dipole} =W_F$	3.0	2.0
Length of dipole	$L_{diopole} = L_{sub}$	42.158	49.0
First dipole distance	d_1	1.044	2.0
The separation between two dipoles	d_2	1.0	1.0
Number of dipoles	N	8 (Unit less)	15 (Unit less)

3.4 FSS distance determination using machine learning ANN model

The application of mathematical concepts to everyday issues has increased in popularity as a result of the increasing capacity for the computation of digital machines and computational methods, both of which have made it simpler to solve lengthy and complicated problems. Putting real-world issues into a mathematical model can improve the representation and solution of certain problems. Nakmouche et al. [44] represents the architecture of the machine learning ANN model. The identification of the most suitable neuron within a neural network relies entirely on the R and mean square error (MSE) values. To determine the ideal neuron and validate the model, the R-value should ideally approach one, indicating a strong correlation, while the MSE value should tend toward zero, signifying minimal error in fitting the data.

This study developed a generalized model that predicted the height of the FSS beneath the antenna using antenna performance parameters. The authors collected a total of 6137 samples to model the parameters, using 70% of the data set for training, 15% for validation, and 15% for testing.

The Levenberg-Marquardt learning algorithm was employed. The authors continue this training process until it reaches saturation. The authors used supervised learning because they had determined the inputs and outputs [45]. Errors propagate back through the neurons during training, leading to adjustments in the neurons' weights. After 316 iterations, the performance diagram as displayed in *Figure 3(a)* and the error histogram as represented in *Figure 3(b)* of training data using the ANN model at a minimum MSE of 0.032844 were obtained. *Table 2* presents the ANN's training progress.

Table 2 Training progress

Unit	Initial Value	Stopped Value	Target Value
Epoch	0	316	1000
Elapsed Time	-	00:00:12	-
Performance	1.62	0.0277	0
Gradient	3.81	0.00495	1e-07
Mu	0.001	1e-08	1e+10
Validation Checks	0	6	6

Figure 4 shows the gradient, momentum, and validation check values obtained during the modeling process for the best-analyzed neural network.

<table>
<tr><td>(a)</td><td>(b)</td></tr>
</table>
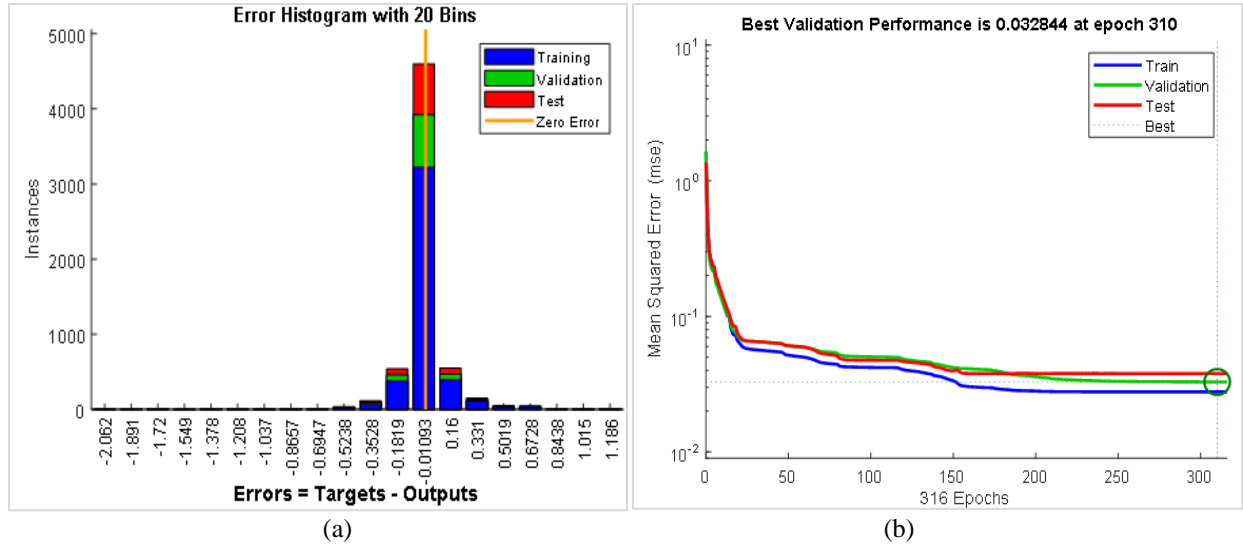
Figure 3 (a) Data performance plots for training, validation, and testing. (b) Error Histogram
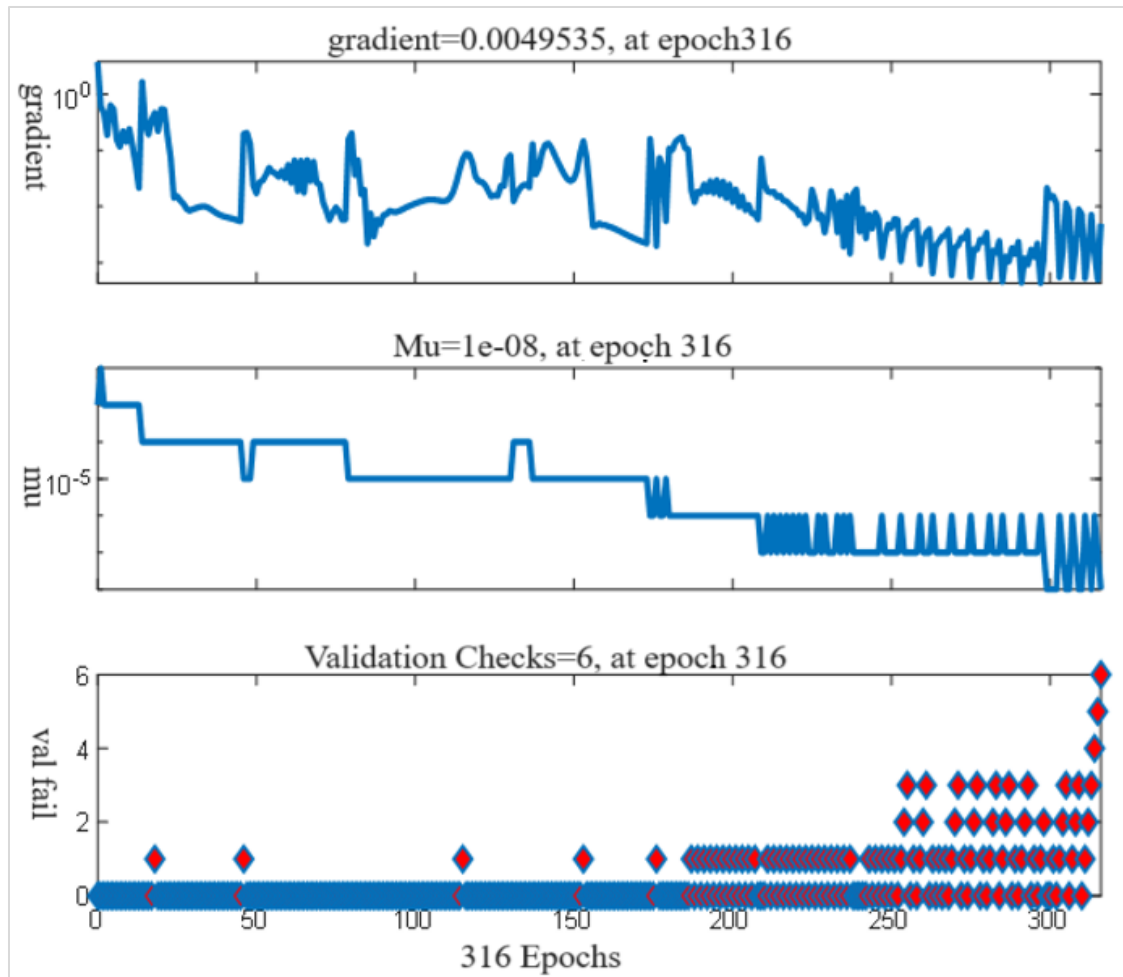
Figure 4 Learning process
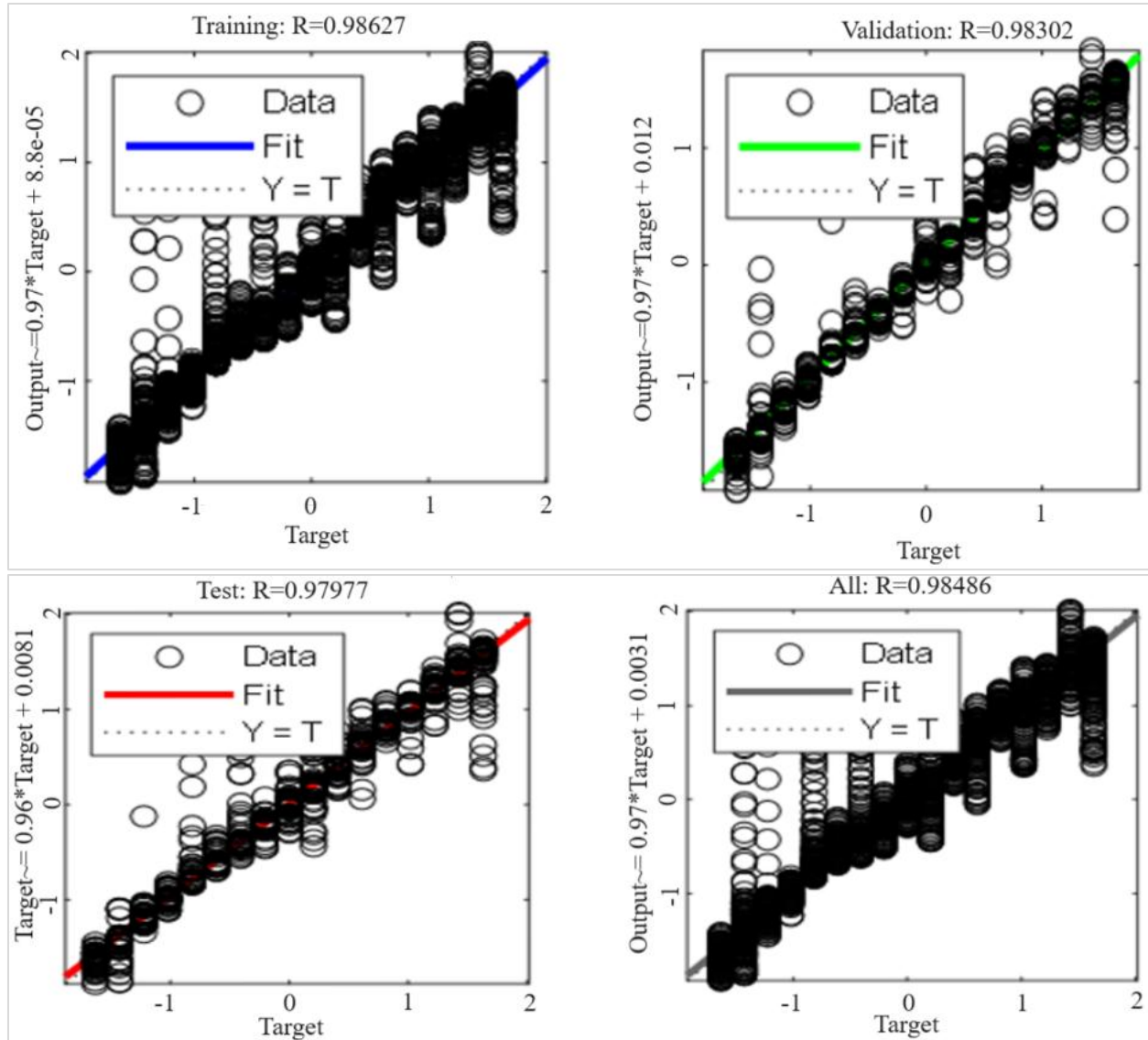
Figure 5 Regression plot

A regression plot is used to evaluate the fitness of input and output data in the structure of the network. A regression plot typically contains four graphs: training, validation, testing, and combining. The regression plots for the considered network are depicted in *Figure 5*. The graph clearly shows that all data sets fit correctly in the line. It shows that the suggested neural network architecture is correct and that it can be used to predict the output, i.e., the height of the FSS below the antenna. The output paths are extremely targeted for training (R^2-value = 0.9868), validation (R^2-value = 0.9830), and testing (R^2-value = 0.9798). These values could imply a total response of R^2-value = 0.9848.

The functional relationship of the output (height) is directly proportional to the performance parameter of the antenna. The functional relationship between the performance parameter of the antenna and the height of FSS can be written in Equation 9.

$$H = f(f_r, S_{11}, VSWR, G) \qquad (9)$$

Where H is the predicted height of the FSS, f_r is resonance frequency (GHz), S_{11} represent the S-parameter/reflection coefficient (dB), VSWR, and gain of the antenna in dB. The data collected from the high-frequency structure simulator (HFSS) simulation is shown in *Table 3*.

Table 3 Data collected from the HFSS simulation

S. No.	Parameter
1	Resonance Frequency(GHz)
2	S-Parameter (dB)
3	VSWR
4	Gain(dB)

Equation 10 can be used to calculate the predicted height of the FSS under the antenna using the ANN algorithm.

$H = 5.15A_1 - 0.10A_2 - 0.20A_3 - 0.34A_4 - 0.94A_5 + 1.45A_6 + 0.16A_7 - 0.97A_8 - 4.41A_9 - 1.27A_{10} - 0.76$ (10)

Where Ai (i=1 to 10) are hidden neuron responses that feed the network output value and can be calculated with Equation 11.

$$\begin{bmatrix} A_1 \\ A_2 \\ A_3 \\ A_4 \\ A_5 \\ A_6 \\ A_7 \\ A_8 \\ A_9 \\ A_{10} \end{bmatrix} = \text{Tangent Sigmoid} \left(\left(\begin{bmatrix} -4.89 & 0.15 & 1.11 & -3.38 \\ 0.08 & -1.59 & 1.45 & -1.76 \\ 2.26 & -0.10 & -8.12 & -4.64 \\ 1.95 & 3.91 & -1.09 & 1.95 \\ -1.15 & -1.33 & -0.23 & 2.97 \\ -2.05 & -1.10 & -0.77 & 2.40 \\ -3.37 & -2.83 & -3.01 & 1.49 \\ 2.37 & -0.20 & 0.55 & 1.45 \\ -3.76 & 0.16 & -0.63 & -4.97 \\ -1.91 & 1.59 & 0.30 & -1.24 \end{bmatrix} \begin{bmatrix} f_r \\ S_{11}[dB] \\ VSWR \\ G[dB] \end{bmatrix} + \begin{bmatrix} 7.29 \\ -2.04 \\ 0.80 \\ -0.25 \\ -0.58 \\ -0.30 \\ 2.10 \\ 0.65 \\ 6.84 \\ -1.86 \end{bmatrix} \right) \right)$$ (11)

Where, Tangent Sigmoid $(x) = \frac{2}{1+e^{-2x}} - 1$ (12)

Where x is any arbitrary value evaluated through a matrix of Equation 11.

R^2-value as 0.999986 having an average absolute percentage error of 0.0124% at 0.0874% root mean square error (RMSE). The training result of the algorithm is shown in *Table 3*. It has been determined that the developed equation represented in Equation 10 is the best for predicting the height of FSS below the antenna.

ANN can predict the outcomes with the highest accuracy. The authors found that the 80/10/10 splitting ratio offered superior performance based on the evaluation metrics they utilized. The authors likely derived this determination from comparative assessments of predictive accuracy, error rates, model robustness, or other relevant performance indicators across the different splitting ratios (70/15/15, 60/20/20).

3.5 Effect of FSS

An inset-feed dual-tuned UWB monopole antenna is first designed at a frequency of 5.5GHz. This antenna has UWB bandwidth from 1.0-9.0GHz (FBW: 145.45%) for a reflection coefficient lower than -10dB while its gain is limited to 4.41 dBi. Then a reflector FSS layer of 15 dipole strip array was arranged at a distance of 8mm beneath the ground of the antenna radiator. It will excellently improve the antenna gain from 4.41dBi to 8.99dBi at the cost of a little decrease in UWB fractional bandwidth(FBW) to 136.73% from 1.12-8.64GHz. The effect of FSS layer attachments is represented in *Figure 6* and showcased in *Table 4*.

Table 4 Effect of FSS

Case / Mode	f_r (GHz)	S_{11} (dB)	-10dB BW (GHz) f_L-f_H	Gain at f_0 (dBi)	-10dB FBW (%)
Without FSS	1.59, 5.77	-15.09, -20.40	1.0-9.0	4.41	145.45
With FSS	1.35, 5.79	-13.03, -18.07	1.12-8.64	8.99	136.73

*f_r=Resonance Frequency; f_0=Design Frequency; FBW=FBW
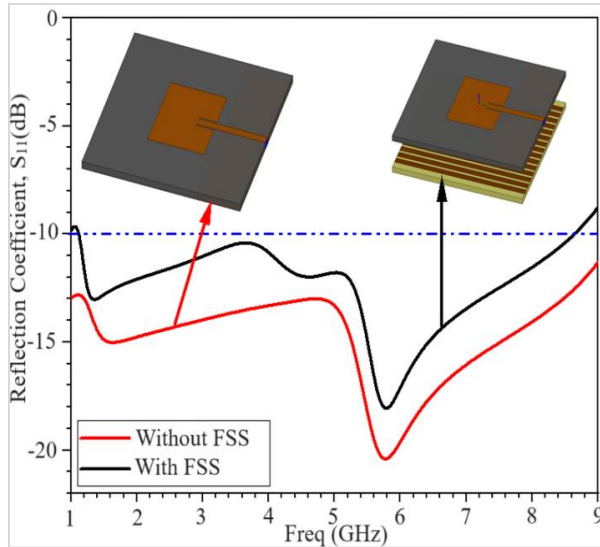
Figure 6 Effect of FSS on the radiator reflection antenna reflection coefficient
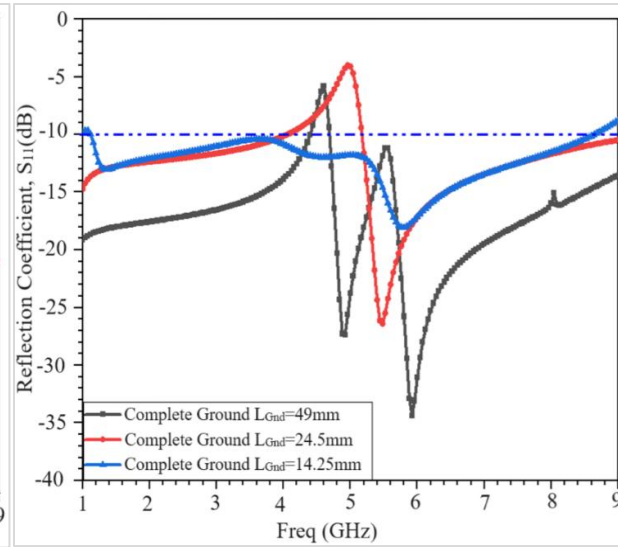
Figure 7 Ground length variation effect on the proposed coefficient

3.6Effect of ground
The ground length is optimized by reducing it from 49mm towards the 50Ω feed line. When the ground surface is fully covered with copper, the antenna achieves dual WB with 792dBi gain at the design frequency. When the length of ground is reduced to 50% i.e., 24.5 mm the gain of the antenna reduces to 5.54 dBi. To maintain the reduced value of gain and make the antenna UWB further reduction of ground length to 14.25 mm yields a gain value of 8.99dBi and UWB from 1.12 GHz to 8.64 GHz. The effect of variation of ground length is illustrated in *Figure 7* and showcased in *Table 5*.

Table 5 Effect of ground

Case / Mode		f_r (GHz)	S_{11} (dB)	-10dB BW f_L-f_H (GHz)	Gain at f_0 (dBi)	Band
Full L_{Gnd}=49mm	Ground	1.0, 1.4.92, 5.93	-19.14, -27.37, -34.36	1.0-4.40, 4.69-9.0	7.92	Dual WB
Ground L_{Gnd}=24.5mm	Length	1.0, 5.47	-14.73, -26.36	1-4.06, 5.17-9.0	5.54	Dual WB
Ground L_{Gnd}=14.25mm	Length	1.35, 5.79	-13.03, -18.07	1.12-8.64	8.99	Single UWB

*f_r=Resonance Frequency; f_0=Design Frequency

Initially, the minimum spacing between the two substrates is equal to quarter-guided wavelength (H=$\frac{\lambda g}{4}$) i.e., 9.97mm with a fixed dipole strip width (W$_{dipole}$) of 2mm. Then it is reduced to a step size of 1mm. All the parametric results of spacing between the two substrates are arranged in *Table 6* and shown in *Figure 8*. It is noticed from *Table 6* that the gain, resonance frequencies (f_r), reflection coefficients (S_{11}), and -10dB BW of the antenna are sensitive to the FSS spacing (H) from the radiating patch. When the FSS spacing is 8.0 mm the antenna achieves the highest gain 8.99dBi at the design frequency (f_0), lowest reflections (-18.07dB), and UWB bandwidth from 1.12GHz to 8.64GHz.

3.7Effect of number of FSS dipole strip width
Initially, the width of each dipole strip is kept equal to the feed width of the rectangular patch (W$_{dipole}$=W$_F$) and the minimum spacing between the two substrates is equal to quarter-guided wavelength (H=$\frac{\lambda g}{4}$) i.e., 9.97mm. Then dipole strip width is reduced to a step size of 0.5 mm without affecting the number of dipole strip elements (N=15). The decrease in strip width size automatically increases the spacing between the dipole strips (d_2) in the same proportion of step size i.e., 0.5 mm. All the parametric sensitivity results of spacing between the two dipole strips and their changes in widths on proposed antenna resonance frequencies (f_r), reflection coefficients (S_{11}), 10dB BW, and antenna

655

gains are shown in *Table 7* and illustrated in *Figure 9*. It has been observed that the gain of the antenna is sensitive to the FSS dipole strip width and spacing and it is highest at 8.99dBi with dipole strip widths of 2.0 mm and their spacing of 1.0 mm. In this complete process, the FSS spacing is kept fixed at 8.0 mm.
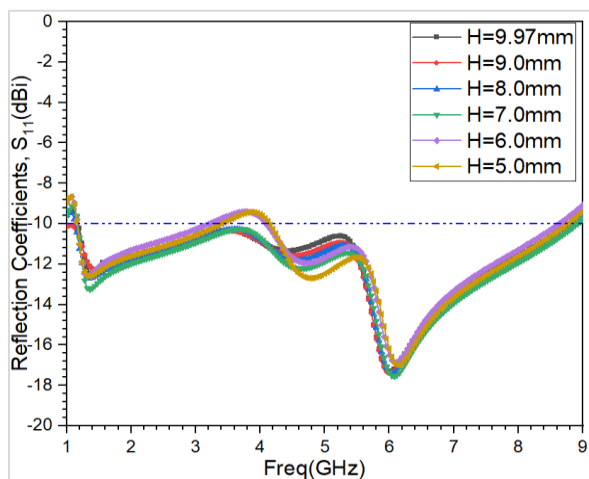
Figure 8 Parametric effect of FSS spacing (H)
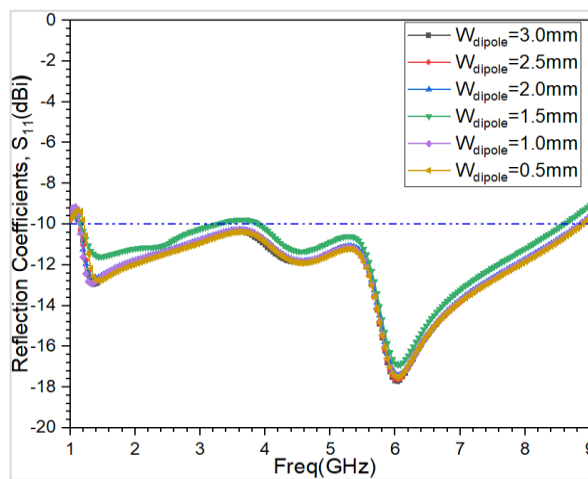
Figure 9 Parametric effect of dipole strip widths and their spacing in FSS

Table 6 Effect of FSS spacing (H)

FSS Spacing (H=$\frac{\lambda_g}{4}$) (in mm)	f_r (GHz)	S_{11} (dB)	-10dB BW f_L-f_H (GHz)	Gain at f_0 (dBi)	Band
H=9.97∼10	1.44, 4.48, 6.0	-12.58, -11.34, -17.32	1.19-8.79, 4.69-9.0	8.29	Single UWB
H=9.0	1.48, 4.50, 6.01	-12.28, -11.58, -17.38	1-8.82	8.50	Single UWB
H=8.0	1.35, 5.79	-13.03, -18.07	1.12-8.64	8.99	Single UWB
H=7.0	1.36, 4.68, 6.08	-13.25, -12.22, -17.55	1.17-8.92	8.59	Single UWB
H=6.0	1.32, 4.72, 6.12	-12.57, -11.95, -16.86	1.17-3.21, 4.09-8.68	8.64	Dual WB
H=5.0	1.36, 4.76, 6.16	-12.61, -12.69, 17.01	1.16-3.40, 4.15-8.77	8.61	Dual WB

Table 7 Effect of dipole strip widths and their spacing in FSS

Strip width, d (mm)	Spacing in strips, d_2 (mm)	f_r (GHz)	S_{11} (dB)	-10dB BW f_L-f_H (GHz)	Gain at f_o (dBi)	Band
3.0	0	1.36, 4.52, 6.04	-12.96, -11.89, -17.72	1.16-8.89	8.54	Single UWB
2.5	0.5	1.40, 4.60, 6.04	-12.76, -11.88, -17.63	1.14-8.87	8.61	Single UWB
2.0	1.0	1.35, 5.79	-13.03, -18.07	1.12-8.64	8.99	Single UWB
1.5	1.5	1.48, 4.55, 6.05	-11.60, -11.34, -16.91	1.16-3.25, 3.90-8.60	8.52	Dual WB
1.0	2.0	1.32, 4.56, 6.05	-12.91, -11.82, -17.49	1.14-8.85	8.53	Single UWB
0.5	2.5	1.45, 4.61, 6.04	-12.77, -11.91, -17.52	1.21-8.88	8.53	Single UWB

3.8Effect of number of dipole strips in FSS

Further, another parametric test with changes in the number of dipole strips (N) with fixed optimized values of the dipole strip widths of 2.0 mm, and the fixed spacing between the substrate and the FSS layer of 8.0 mm is carried out. The number of dipole strips could be increased from 9 to 19 by the decrease in

dipole strip spacing (d2) in a step size of 0.5 mm. The number of dipole strips also affects the antenna gain as well as the other resultant parameters as showcased in *Table 8* and illustrated in *Figure 10*. It is recorded that the minimum reflections and highest gain values were achieved with the 15 dipole strips.
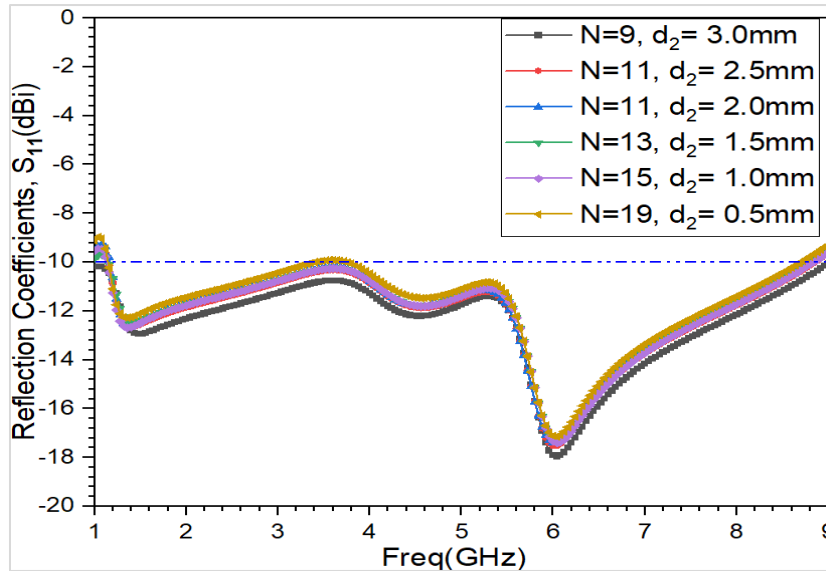
Figure 10 Parametric effect of the number of dipole strips in FSS

Table 8 Effect of number of dipole strips in FSS

Number of dipole strips (N)	Spacing in strips (d_2)	f_r (GHz)	S_{11} (dB)	-10dB BW f_L-f_H (GHz)	Gain at f_o (dBi)	Band
N=9	3.0	1.48, 4.56, 6.04	-12.95, -12.21, -17.96	1.0-9.0	8.50	Single UWB
N=11	2.5	1.40, 4.56, 6.0	-12.65, -11.87 -17.51	1.15-8.85	8.62	Single UWB
N=11	2.0	1.36, 4.53, 6.0	-12.63, -11.80 -17.39	1.17-8.82	8.56	Single UWB
N=13	1.5	1.40, 4.56, 6.04	-12.48, -11.78, -17.35	1.15-8.83	8.55	Single UWB
N=15	1.0	1.35, 5.79	-13.03, -18.07	1.12-8.64	8.99	Single UWB
N=19	0.5	1.36, 4.60, 6.04	-12.28, -11.47, -17.14	1.15-3.41, 3.76-8.70	8.60	Dual WB

4 Results

The fabricated FSS antenna is measured, analyzed, and discussed in detail in the forthcoming sub-sections.

4.1 Fabrication and Measurements of Fabricated Proposed Antenna Prototype

A double-layered antenna is fabricated and measured. The antenna radiator patch and ground are fabricated on a low-loss RT Duroid 5880 substrate while the

reflector FSS with 15 dipole strips is etched on a single-sided low-cost FR4 substrate. Finally, the reflector and radiator are connected at a separation of 8.0 mm with the help of four cylindrical plastic materials. The fabricated radiator, ground, and reflector FSS are displayed in *Figure 11 (a-d)*. The following are the common steps involved in the fabrication of the radiator and reflector elements of the antenna;

-A piece of 1.588mm thick RT double-sided copper-clad RT Duroid 5880 substrate of dimensions 49mm×49mm is cut using a printed circuit board (PCB) cutter machine for the radiator fabrication, while another piece of 1.6mm thick FR4 single-sided copper-clad substrate of the same dimension is cut for the reflector fabrication.

-Two negatives (one for the antenna radiator and the other for the reflector) with the same dimensions as the PCB pieces are prepared by artwork using black film.

-By repeating the above step third negative is also prepared (for the ground with 49mm×49mm) just the back side of the radiator of the RT Duroid 5880 substrate.

-Then these negatives are put on the clear RT Duroid and FR4 pieces and ultra-voilet (UV) rays are exposed for 30 seconds for image development of the radiator, ground, and reflector.

-After that these PCB pieces are dropped in the photo developer solutions.

-Further, these two PCB pieces fall into a blue-die solution.

- At last, these blue-die PCB pieces are hung in the $FeCl_3$ solution, for a sufficient time until the undesired copper has been removed from the radiator and reflector pieces.

-After the completion of the etching process a 50Ω subminiature version A (SMA) connector is soldered

in the feed of the radiator and 4-pieces of 8mm-height plastics (used as the separator) are pasted using a glue bond between the antenna reflector and radiator.

The proposed antenna reflection coefficient was generated from the simulation and measured using Agilent Technologies N5247A vector network analyzer (VNA). In the measurement setup, a VNA with a maximum operating frequency of 67 GHz is employed for measuring frequency-dependent parameters such as the reflection coefficient (VSWR/Impedance). These measurements are conducted using the sweep frequency mode. To measure antenna-related parameters like gain and efficiency, an in-house semi-automated anechoic chamber is utilized. This chamber is equipped with a stepper motor-controlled 2-axis position, a standard gain-calibrated broadband antenna, and a power meter. The far-field experimental setup is utilized for the proposed antenna structure. In this setup, the antenna under test and a calibrated antenna are positioned approximately more than three times of guided wavelength i.e., 120 mm apart to achieve the required far-field distance within the operating frequency range of 1 GHz to 9 GHz as displayed in *Figure 11(e).* Typically, a 3.5 mm SMA connector is used in conventional designs for the lower frequency range of operation (DC to 18 GHz).

(a)　　　　　　　(b)　　　　　　　(c)

(c)
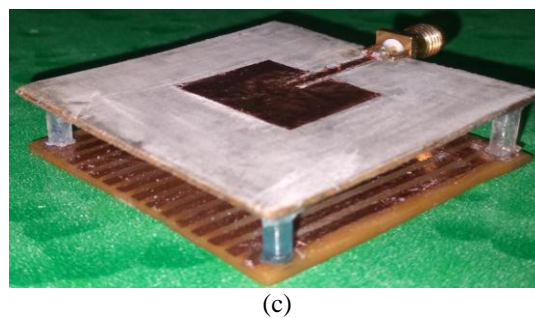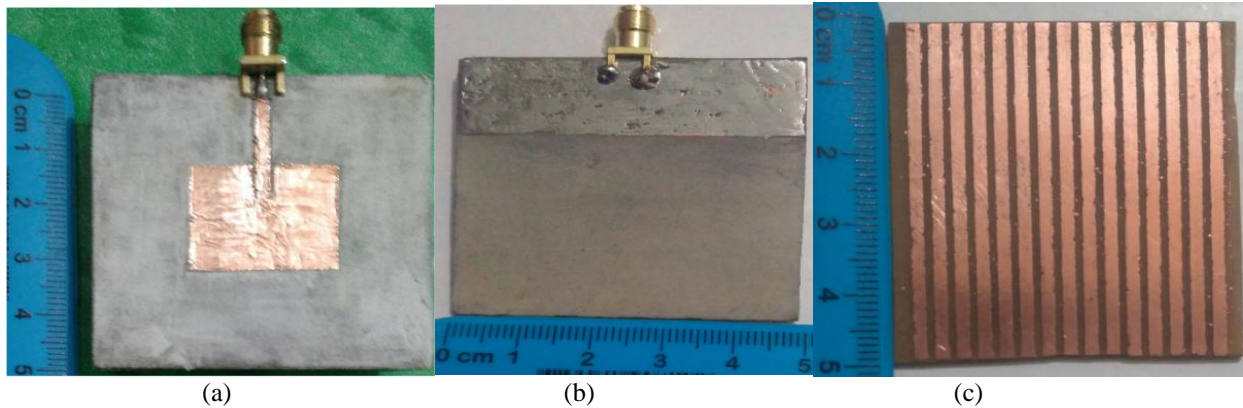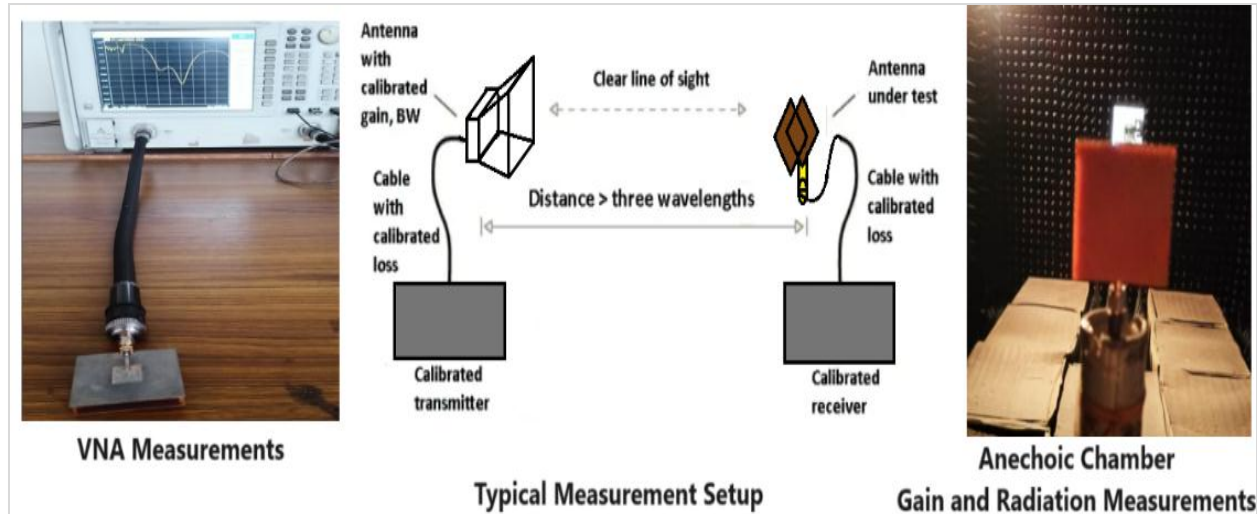
(e)

Figure 11 Fabricated antenna views (a) Top patch radiator, (b) Bottom ground, (c) FSS reflector, and (d) Proposed Antenna prototype model (e) Calibration and measurement setup

4.2Reflection coefficient

The comparison plots of the simulated and measured reflection coefficient are plotted in *Figure 12*. It is concluded from the measured plot that it follows the simulated reflection coefficient curve and a small reduction in the FBW is observed from the simulated reflection coefficient curve. The measured curve has a UWB range from 1.10GHz to 8.21GHz (FBW: 129.27%) while the simulated curve UWB performance in the span of 1.12GHz to 8.64GHz (FBW: 136.73%). The resonance frequencies in the simulated plot are 1.35GHz and 5.79GHz while those in the measured plot are 1.41GHz and 6.01GHz respectively. Therefore, both simulated and measured plots are an excellent match with each other as illustrated in *Figure 12* and showcased in *Table 9*. The slight variations from the ideal dimensions and fabrication tolerances are the main reason of deviations in resonance frequency and FBW. Another reason for the variations in the antenna performance is its practical air spacing between the radiator and reflector while pasting of 4-plastic separators. The other reasons for the discrepancies in the measured data are environmental factors and operational conditions of the antenna. The environmental factor mainly includes temperature and humidity. These factors may slightly change the conductivity, effective permittivity, and loss tangent of the PCB materials. The changes in these factors may result in deviation in frequency shift as well as compression and expansion of the FBW noticed. When an antenna operates in an environment where small

objects are present in its near-field reason, then it undergoes multiple reflections and interferences from these objects hence, these degrade the reflection coefficient value and increase interference changes in frequency and bandwidth.

4.3Antenna gain

The antenna gains without the FSS reflector and with the FSS reflector are drawn in *Figure 13*. It is observed from the comparison that 2.80GHz to 7.40GHz the antenna gain is excellently enhanced in the frequency sweep from 2.80 GHz to 7.40 GHz. This reaches its peak value of 9.85 dBi at a frequency of 6.0 GHz with an FSS reflector while the peak gain value without a reflector was 4.41 dBi at 5.79 GHz. At the designed frequency of 5.5GHz, the gains of the antenna with an FSS reflector and without an FSS reflector are 4.41 dBi and 8.99 dBi respectively. The proposed antenna gain measurements are carried out in an anechoic chamber which is displayed in the left corner of the gain comparison plots.

4.4Radiation pattern

The gain radiation pattern of the proposed antenna without and with an FSS reflector in the E-plane and H-plane with Φ=0° and Φ=90° are displayed in *Figure 14*. It is observed from the radiation pattern that the antenna without a reflector surface beneath the radiator ground the radiation in the E-plane is omnidirectional and in the H-plane it resembles the figure of eight shapes. After the introduction of the reflector beneath the ground of the radiating patch the bidirectional nature of the radiation pattern becomes

almost unidirectional in E-plane with a FBR of 17.5 dB. The back lobe is almost diminished in the E-plane. While in the H-plane back lobe becomes

weaker front to back lobe ratio in the H-plane is 15.2 dB.

Table 9 Simulated and measured reflection coefficients

Case / Mode	f_r (GHz)	S_{11} (dB)	-10dB BW (GHz)	f_L-f_H	Gain at f_0(dBi)	-10dB FBW(%)
Simulated With FSS	1.35, 5.79	-13.03, -18.07	1.12-8.64		8.99	136.73
Measured With FSS	1.41, 6.01	-15.06, -19.03	1.10-8.21		9.85	129.27
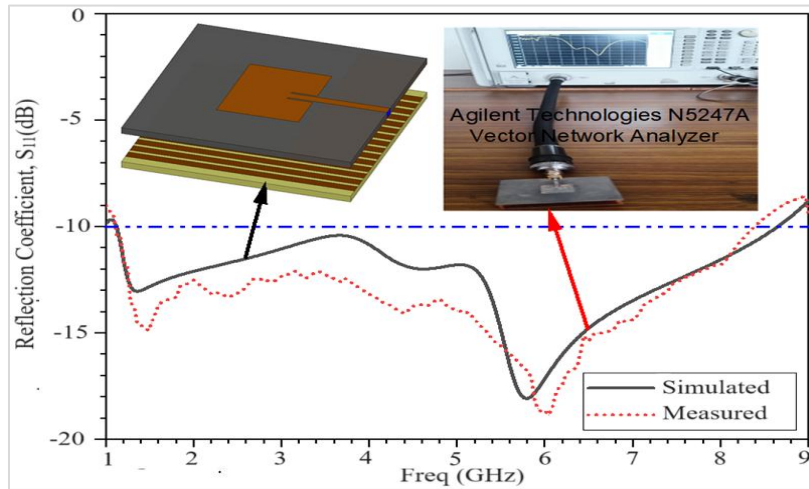
Figure 12 Simulated and measured reflection coefficient curve
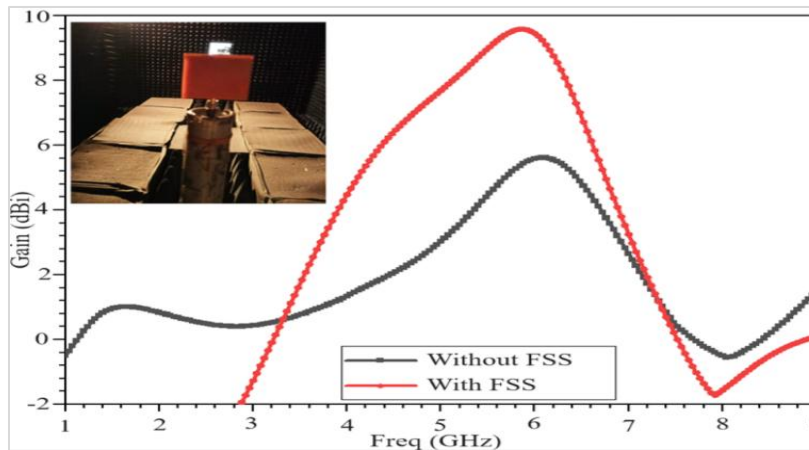
Figure 13 Antenna gain plots without FSS reflector and with FSS reflector

The gain radiation pattern of the proposed antenna simulated and measured in the E-plane and H-plane with Φ=0° and Φ=90° are compared in *Figure 15*. It is noticed from the radiation patterns when the radiation pattern plot in the E-plane is similar to the measured radiation plot. Both have a small back lobe as compared to the main lobe. The peak value of the main lobe coincides and the measured radiation

pattern follows the simulated radiation pattern in the main lobe direction. In H-plane the measured radiation pattern is not exactly match the simulated one. The reason for these discrepancies in the measured data is due to an error in the measurement setup or some measurement and observation errors and one most important responsible parameter in its fabrication is SMA connector soldering errors.

660

(a)   (b)
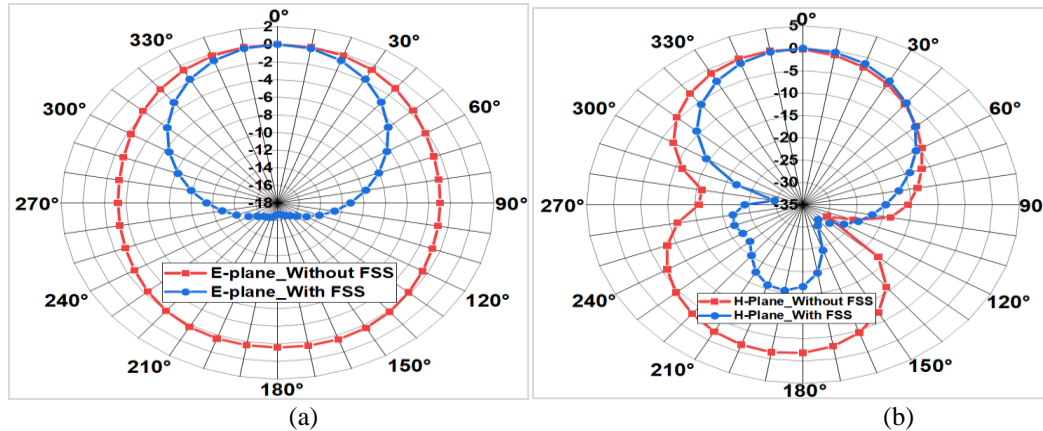
Figure 14 E-pane and H-plane Radiation Patterns without FSS and with FSS @ 5.50GHz

(a)   (b)
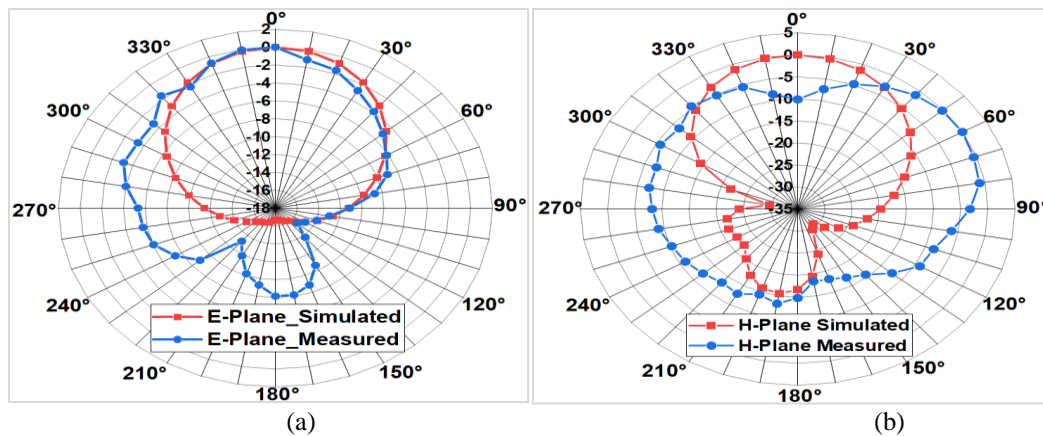
Figure 15 Simulated and measured E-pane and H-plane radiation patterns with FSS @5.50GHz

4.5 Equivalent circuit and its validation

The equivalent circuit of the proposed antenna with an FSS reflector is developed from the reflection coefficient plot obtained from the HFSS simulation. As per the RLC resonance circuit theory, the lowest impedance represents the series RLC connection while the highest magnitude of impedance represents the parallel combination of RLC circuits [4, 44, 45]. There are three resonance frequencies 1.35GHz, 4.61GHz, and 5.79GHz in the UWB range from 1.12GHz to 8.64GHz corresponding to the lowest reflection coefficient values at these frequencies. The impedances at these frequencies are (4.32+j35.44) Ω, (8.61+j34.54) Ω, and (1.13+j10.25) Ω respectively. These are very close to zero values and talk about the three series RLC circuits in parallel branches as shown in *Figure 16*. The values of the R, L, and C

parameters for each resonance branch are evaluated using the basic bandwidth and quality factor relationships [44, 45]. The evaluated values retune with the help of ADS software for the validations of the HFSS reflection coefficient generated circuit. According to references 1 and 2, the reflection coefficient values of the ADS software are shown in *Figure 17(a)*. This plot is then compared with the HFSS simulated value. It is noticed that both ADS and HFSS S_{11} plots have almost similar resonance frequencies and bandwidth, also following the shapes as depicted in *Figure 17(b)*. The existing error margins in the resonance frequencies are marked with black and red dash-dot lines. This validated the generated RLC electrical equivalent circuit of the designed antenna.
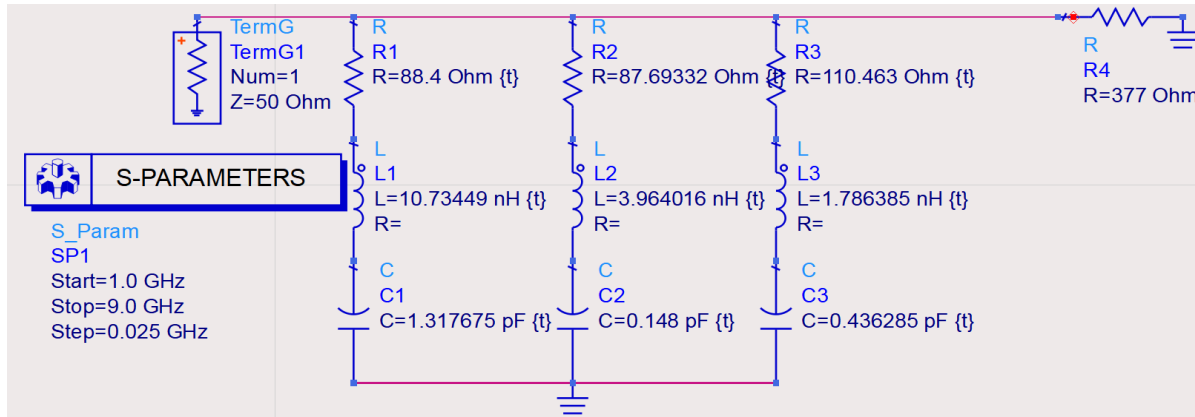
Figure 16 RLC electrical equivalent of the Proposed FSS reflector antenna

(a)   (b)
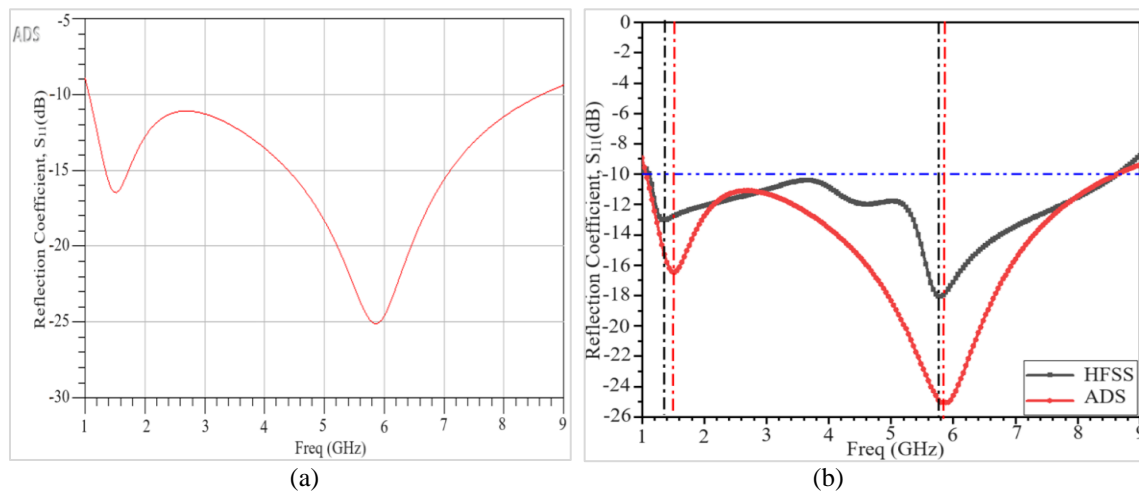
Figure 17 Reflection coefficient plot (a) ADS software-generated, (b) Its validations

5. Discussion

To improve control over electromagnetic waves that are reflected and transmitted from the FSS can also be used in antenna as a reflector. ANN machine learning method is utilized to determine the optimum distance of the FSS reflector beneath the radiating substrate. The proposed antenna is simple in structure with 15 dipole strips at a distance of 8mm beneath the ground and is used as a reflector resulting in UWB bandwidth from 1.12GHz to 8.64GHz and achieving a gain enhancement of 4.58dBi (from 4.41dBi to 8.99dBi). The 8.0 mm air gap reduces the overall volume of the antenna. The FSS reflector layer strip width, strip distances, and air gap between the main and FSS substrate help to enhance the gain of the antenna while the overall bandwidth of the antenna is improved by a reduction in the length of the antenna. The FSS layer also improves the radiation characteristics and directional properties in its E-plane and H-planes. The measured results

validate the prototype results with simulated results comparisons. The RLC electrical equivalent circuit of the antenna is manually evaluated and validated in the ADS software by comparing the reflection coefficients plots.

5.1 Comparison with existing literature

The proposed antenna resultant parameters are compared with the existing similar antennas and other techniques used for gain enhancements. The parameter comparison of the FSS reflector rectangular antenna 'show' that the antenna resonates at a frequency of 5.80GHz and 1.35GHz within the UWB range from 1.12GHz-8.64GHz while all other antenna has multi-band narrow bandwidth or wide bandwidths. In most cases, the radiator and reflector FSS surface are fabricated on the same substrate except in the proposed design, and in reference 35, the radiator and reflector are fabricated on two separate substrates. The complexity of the FSS layer is reduced in the proposed design as compared to

662

reference 35 by reducing the number of dipole strips in the array and increasing the separation between the two dipole strips. Previously published antennas cover a limited number of sub-6GHz band applications while the proposed antenna covers the whole range of the sub-6GHz band including important 5G bands n77, n78, and n79. The resultant performance parameters comparison between the proposed antenna and the existing antenna models found in the literature are presented in *Table 10*. In the literature, the comparisons table shows that the suggested antenna design has a maximum improvement of gain of 4.52dBi, which is significantly superior to the gains of the existing antennas except for references [35, 46–48]. A comparison with active similar antennas in the literature has been presented and shows that the present design is simpler, easy to fabricate, has UWB bandwidth, and has higher gain than the earlier studies.

A complete list of abbreviations is listed in Appendix I.

Table 10 Comparison of the proposed antenna and with similar published FSS/metasurface work

Ref. No.	Ant. Size (mm³) (Ant. Type)	Design Freq., f₀ (GHz)	Method for Gain Enhancement	FBW fL-fH, (GHz)	Complexity	Gain (dBi)	Gain Enhancement (dBi)	Cost	Efficiency (%)
Tahir et al.[6] 2021	66.4×66.4 × 1.6, FR-4 (Monopole)	2.45	SRR triplet (without reflector)	1.81-3.0	Moderate	7.16	7.286 to 7.16	Low	92.85
Belen,[17] 2018	63.65×54.16 × 1.588, FR-4	2.4	Band-Pass FSS (Double Layer)	2.4	High	7	5 to 7	Low	NG
Bhattacharya et al.[23], 2020	40 × 30 × 0.8 (DR height = 4.3 mm)	8.15–13.2 (5.05)	FSS (Double side)	8.15–13.2 (5.05)	High	7.8	3.3 to 7.8	High	NG
Hussain, et al.[24], 2023	32 × 25 × 1.52 (Rogers RT/Duroid 6002)	12.0	FSS at a distance of 9.0mm	5-18	Moderate	10.5	6.5-10.5	High	>78
Tewary et al.[27] 2023	20×14 ×1.6 FR4 (Monopole)	9.12	6×6 (39mm× 39mm) FSS layer beneath the antenna at a 15mm distance	9.12-31.67 (WB)	Moderate	9.40	3.90 to 9.40 (5.5)	Low	58
Tewary et al. [28]2022	26×26 ×1.6 FR4 (Monopole)	2.75	4×4 (56mm× 56mm) FSS layer beneath the antenna at a 26.2mm distance	2.75-28 (SWB)	Moderate	9.40	4.80 to 9.30 (3.5)	Low	76
Ara and Nunna [37]. 2023	49 ×49 ×1.588 RT Duroid 5880 and FR4 (Monopole)	5.8	49 number of Dipole strips FSS as a reflector at a distance of 8 mm (Double Layer)	3.91-6.44 (WB)	Moderate	7.76	2.87 to 7.76	Medium	>88
Belen, et al.[48] 2020	50 × 53.4 × 1.6 (FR-4)	2.4	DRA-FSS at a distance of 16 mm	2.4	Low	8.6	3 to 8.6	Low	NG

Ref. No.	Ant. Size (mm³) (Ant. Type)	Design Freq., f_0 (GHz)	Method for Gain Enhancement	FBW f_L-f_H, (GHz)	Complexity	Gain (dBi)	Gain Enhancement (dBi)	Cost	Efficiency (%)
Patel and Raval [49] 2021	60× 50 × 1.6 (FR-4)	5.8	SIW Cavity Backed antenna using two dielectric resonator loading, FR4 inner cylinder, Teflon outer cylinder	5.7-5.9	High	8.13	3.13 to 8.13	Low	NG
Jing et al. [50] 2023	50.4× 28 × 0.1 Polyimide (PI) substrate	2.4	3×3 (102mm ×102mm) rotatable curved FSS	2.18-2.90 ((NB)	High	8.31	3 to 8.31	Medium	NG
Ghosh, et al. [51] 2016	60 × 60 × 1.6 FR-4	3.75,5.98 and 8.79 (Multi-band)	AMC (Double Layer)	Multi-band, 3.75, 5.98 and 8.79	High	7.52	3.88 to 4.93	Low	NG
Belabbas et al. [52] 2021	20× 20 × 1.6 RT Duroid TTN	28.4	Asymmetric 8×8 AMC ground plane (Impedance surface)	28.4-36	Low	8.30	4 to 8.3	High	92
Proposed	49×49 x1.588 RT Duroid 5880 and FR4 (Monopole)	5.5	15 number of Dipole strips FSS as a reflector	1.12-8.64 (UWB)	Least	8.99	4.41 to 8.99 (4.58dBi)	Medium	97

*NB=Narrow band; WB=Wide Band; UWB=Ultra-Wideband; NG=Not Given

5.2 Limitation

The projected antenna has UWB, is simple, compact in size, has high gain, and very high radiation efficiency values although it has quite a few limitations. As the reflector FSS surface is applied beneath the bottom at a distance of an 8.0 mm gap, this increases the volume of the antenna and therefore it engages more volume instead of area. Since the radiating patch is etched on the RT Duroid 5880 top layer, consequently the antenna becomes expensive. The dipole strip array FSS enhances the gain and radiation efficiency but compresses the reflection coefficient. As the antenna has UWB bandwidth from 1.12GHz to 8.64GHz it is appropriate to Sub 6GHz communications like n46 (5150-5925MHz), n47 (5855-5925MHz), n77 (3900-4200MHz), n78(3300-3800MHz), n79 (4400-5000MHz), n96/n102 (5925-6425MHz) etc bands. However, the UWB bandwidth results in the interferences with other than 5G

applications such as from the Wi-Fi/Bluetooth/WLAN (2.4-2.5GHz), Wi-MAX (3.5GHz), CDMA (1700/1900/2100MHz), GSM (1850-1990MHz), ISM (2.4-2.4835 GHz), PCS (1850-1990 MHz) bands, Wi-Fi5/6 (5 GHz), LTE (2.3 GHz, 2.5 GHz, and 5.8GHz), HiperLAN (5.15-5.35GHz), and another microwave L-band, S-band, C-band for wireless, RADAR and satellite applications. The size of the main radiator is wider as compared to the other work of the same domains so need to modify this in the future. In most of the work complex geometries were fabricated, which are difficult to manufacture. In the proposed learning different substrates are utilized for both the patch and the FSS design and simple thick strip lines with reduced number of counts were used for the assembly of the FSS.

6. Conclusion and future work

The projected antenna has UWB, excellent gain, and very high radiation efficiency values although it has few limitations. As the FSS surface is set beneath the bottom ground at some gap, increases the antenna volume in the third dimension and hence will occupy more space. Since the main rectangular patch antenna is designed on the RT Duroid 5880, make the antenna expensive. The introduced FSS reduced the reflection coefficient but improved the gain and radiation efficiency. The proposed antenna has FBW 136.73% from 1.12GHz to 8.64GHz, it is the better choice to use for all Sub-6GHz applications including important n77(3300 – 4200GHz), n78 (3300 – 3800MHz), n79 (4400 – 5000MHz) bands, etc along with code division multiple access(CDMA) (1700/1900/2100MHz), GSM (1850-1990MHz), ISM (2.4-2.4835 GHz), PCS (1850-1990 MHz) bands, Wi-Fi 4/5/6 (2.4 GHz and 5 GHz), WLAN (2.5GHz), Bluetooth (2.45GHz), LTE/Wi-MAX (2.3, 2.5 and 5.8GHz), HIPERLAN (5.15-5.35GHz), and another microwave L-band, S-band, C-band for wireless, RADAR and satellite communications. In most of the literature complex geometries were fabricated on the same substrate material, also the same substrate was used for the radiator as well as the FSS structure, which are difficult to manufacture. In the proposed study different substrates are used for rectangular patches as well as for the FSS design and simple equally spaced low count of dipole lines were used for the construction of the FSS. In the future there is the need to reduce the size of the antenna. The UWB bandwidth covers applications other than 5G, this generates chances of interference with additionally covered applications. Therefore, it is desired to reduce the interference by narrowing the bandwidth. This could be done by changing the air gap between the two substrates and making the FSS layer tuneable by using PIN diodes (BAR64-02V) and increasing the length of the ground surface.

Conflicts of interest

The authors have no conflicts of interest to declare.

Data availability

None.

Author's contribution statement

Shabnam Ara: Conceptualization, investigation, writing – original draft, writing – review and editing. **Dr. Prasanthi Kumari Nunna:** Study conception, design, supervision, investigation of challenges, and draft manuscript preparation.

References

[1] Howell J. Microstrip antennas. IEEE Transactions on Antennas and Propagation. 1975; 23(1):90-3.

[2] Bansal A, Gupta R. A review on microstrip patch antenna and feeding techniques. International Journal of Information Technology. 2020; 12(1):149-54.

[3] Varshney A, Sharma V, Nayak C, Goyal AK, Massoud Y. A low-loss impedance transformer-less fish-tail-shaped MS-to-WG transition for K-/Ka-/Q-/U-band applications. Electronics. 2023; 12(3):1-21.

[4] Varshney A, Sharma V, Elfergani I, Zebiri C, Vujicic Z, Rodriguez J. An inline V-band WR-15 transition using antipodal dipole antenna as RF energy launcher@ 60 GHz for satellite applications. Electronics. 2022; 11(23):1-16.

[5] Yuan N, Yeo TS, Nie XC. A fast analysis of scattering and radiation of large microstrip antenna arrays. IEEE Transactions on Antennas and Propagation. 2003; 51(9):2218-26.

[6] Tahir FA, Arshad T, Ullah S, Flint JA. A novel FSS for gain enhancement of printed antennas in UWB frequency spectrum. Microwave and Optical Technology Letters. 2017; 59(10):2698-704.

[7] Monavar FM, Komjani N. Bandwidth enhancement of microstrip patch antenna using Jerusalem cross-shaped frequency selective surfaces by invasive weed optimization approach. Progress in Electromagnetics Research. 2011; 121:103-20.

[8] Mahfuz MH, Islam MR, Habaebi MH, Sakib N, Hossain AZ. A notched UWB microstrip patch antenna for 5G lower and FSS bands. Microwave and Optical Technology Letters. 2022; 64(4):796-802.

[9] Parkvall S, Dahlman E, Furuskar A, Frenne M. NR: the new 5G radio access technology. IEEE Communications Standards Magazine. 2017; 1(4):24-30.

[10] Yuan Y, Xi X, Zhao Y. Compact UWB FSS reflector for antenna gain enhancement. IET Microwaves, Antennas & Propagation. 2019; 13(10):1749-55.

[11] Neebha TM, Andrushia AD, Malin BP, Varshney A, Manjith R, Dhanasekar S. On the design of miniaturized C-shaped antenna based on artificial transmission line loading technique. Journal of Electromagnetic Waves and Applications. 2023; 37(6):814-26.

[12] Patel A, Mewada H, Vala A, Patel S, Chauhan D, Patel P. Superstrate microstrip antenna for 5G wireless communication applications. In international conference on optical and wireless technologies 2021 (pp. 125-32). Singapore: Springer Nature Singapore.

[13] Ali M, Arya RK, Yerrola AK, Murmu L, Kumar A. Bandwidth and gain enhancement with cross-polarization suppression in microstrip antenna with

superstate. In XXXIVth general assembly and scientific symposium of the international union of radio science 2021 (pp. 1-4). IEEE.

[14] Kim JH, Ahn CH, Bang JK. Antenna gain enhancement using a holey superstrate. IEEE Transactions on Antennas and Propagation. 2016; 64(3):1164-7.

[15] Vardaxoglou JC. Frequency selective surfaces: analysis and design. Research Studies Press, Wiley; 1997.

[16] Nakmouche MF, Allam AM, Fawzy DE, Lin DB. Development of a high gain FSS reflector backed monopole antenna using machine learning for 5G applications. Progress in Electromagnetics Research M. 2021; 105:183-94.

[17] Belen MA. Performance enhancement of a microstrip patch antenna using dual-layer frequency-selective surface for ISM band applications. Microwave and Optical Technology Letters. 2018; 60(11):2730-4.

[18] Sarkhel A, Bhadra CSR. Enhanced-gain printed slot antenna using an electric metasurface superstrate. Applied Physics A. 2016; 122:1-11.

[19] Fernandes EM, Da SMW, Da SBL, De SCAL, De AHX, Casella IR, et al. 2.4–5.8 GHz dual-band patch antenna with FSS reflector for radiation parameters enhancement. AEU-International Journal of Electronics and Communications. 2019; 108:235-41.

[20] Tilak GB, Kotamraju SK, Madhav BT, Kavya KC, Rao MV. Dual sensed high gain heart shaped monopole antenna with planar artificial magnetic conductor. Journal of Engineering Science and Technology. 2020; 15(3):1952-71.

[21] Gharsallah H, Osman L, Latrach L. Circularly polarized two-layer conical DRA based on metamaterial. Microwave and Optical Technology Letters. 2017; 59(8):1913-9.

[22] Ram KRV, Kumar R. Slotted ground microstrip antenna with FSS reflector for high-gain horizontal polarisation. Electronics Letters. 2015; 51(8):599-600.

[23] Bhattacharya A, Dasgupta B, Jyoti R. Design and analysis of ultrathin X-band frequency selective surface structure for gain enhancement of hybrid antenna. International Journal of RF and Microwave Computer-Aided Engineering. 2021; 31(2):e22505.

[24] Hussain M, Sufian MA, Alzaidi MS, Naqvi SI, Hussain N, Elkamchouchi DH, et al. Bandwidth and gain enhancement of a CPW antenna using frequency selective surface for UWB applications. Micromachines. 2023; 14(3):1-13.

[25] Ranga Y, Matekovits L, Esselle KP, Weily AR. Multioctave frequency selective surface reflector for ultrawideband antennas. IEEE Antennas and Wireless Propagation Letters. 2011; 10:219-22.

[26] Devarapalli AB, Moyra T. Design of a metamaterial loaded W-shaped patch antenna with FSS for improved bandwidth and gain. Silicon. 2023; 15(4):2011-24.

[27] Tewary T, Maity S, Roy A, Bhunia S. Wide band microstrip patch antenna with enhanced gain using FSS structure. Journal of Microwaves, Optoelectronics and Electromagnetic Applications. 2023; 22:329-45.

[28] Tewary T, Maity S, Mukherjee S, Roy A, Sarkar PP, Bhunia S. High gain miniaturrized super-wideband microstrip patch antenna. International Journal of Communication Systems. 2022; 35(11):e5181.

[29] Tewary T, Maity S, Mukherjee S, Roy A, Sarkar PP, Bhunia S. FSS embedded high gain 'N'shaped miniaturized broadband antenna. AEU-international Journal of Electronics and Communications. 2023; 158:154465.

[30] Prasad N, Pardhasaradhi P, Madhav BT, Islam T, Das S, El GM. Radiation performance improvement of a staircase shaped dual band printed antenna with a frequency selective surface (FSS) for wireless communication applications. Progress in Electromagnetics Research C. 2023; 137:53-64.

[31] Renit C, Raj TA. Wearable frequency selective surface-based compact dual-band antenna for 5G and Wi-Fi applications. Automatika. 2024; 65(2):454-62.

[32] Lanka MD, Chalasani S. M-shaped conformal antenna with FSS backing for gain enhancement. Engineering Proceedings. 2024; 59(1):1-10.

[33] Al-qutbi MM. Design and analysis of microstrip antenna with frequency selective surface superstrate. Master's Thesis, Altınbaş University, Graduate Education Institute, Istanbul. 2023.

[34] Danuor P, Moon JI, Jung YB. High-gain printed monopole antenna with dual-band characteristics using FSS-loading and top-hat structure. Scientific Reports. 2023; 13(1):1-12.

[35] Tariq S, Hussain Q, Alzaidi MS, Ghoniem RM, Alibakhshikenari M, Althuwayb AA, et al. Frequency selective surfaces-based miniaturized wideband high-gain monopole antenna for UWB systems. AEU-International Journal of Electronics and Communications. 2023; 170:154841.

[36] Hossain T, Chakraborty S, Uddin MJ, Gafur A, Rashid SZ, Rahman MA, et al. Performance enhancement of UWB antenna using FSS layer for millimeter-wave 5G. In international conference on next-generation computing, IoT and machine learning 2023 (pp. 1-6). IEEE.

[37] Ara S, Nunna PK. Gain enhancement of a monopole antenna using frequency selective surface for sub-6 GHz band applications. International Journal of Advanced Technology and Engineering Exploration. 2023; 10(104):840-57.

[38] Yi X, Zhou L, Hao S, Chen X. Dual-band high-gain shared-aperture antenna integrating fabry-perot and reflectarray mechanisms. Electronics. 2022; 11(13):1-10.

[39] Decoster B, Maes S, Cuiñas I, García SM, Caldeirinha R, Verhaevert J. Dual-band single-layer fractal frequency selective surface for 5G applications. Electronics. 2021; 10(22):1-16.

[40] Al-gburi AJ, Ibrahim IM, Zakaria Z, Abdulhameed MK, Saeidi T. Enhancing gain for UWB antennas using FSS: a systematic review. Mathematics. 2021; 9(24):1-16.

[41] Qin PY, Ji LY, Chen SL, Guo YJ. Dual-polarized wideband fabry-pérot antenna with quad-layer partially reflective surface. IEEE Antennas and Wireless Propagation Letters. 2018; 17(4):551-4.

[42] Chang K. RF and microwave wireless systems. John Wiley & Sons; 2004.

[43] Balanis CA. Antenna theory: analysis and design. John Wiley & sons; 2016.

[44] Nakmouche MF, Allam AM, Fawzy DE, Lin DB. Low profile dual band H-slotted DGS based antenna design using ANN for K/Ku band applications. In 8th international conference on electrical and electronics engineering 2021 (pp. 283-6). IEEE.

[45] Sarabakha A, Imanberdiyev N, Kayacan E, Khanesar MA, Hagras H. Novel levenberg–marquardt based learning algorithm for unmanned aerial vehicles. Information Sciences. 2017; 417:361-80.

[46] Varshney A, Sharma V, Kumar R. Microstrip interconnect design and modeling using reverse approach to obtain an efficient wideband MS line-to-RWG hybrid transition. In printed antennas 2022 (pp. 67-80). CRC Press.

[47] Varshney A, Sharma V, Srivastava A. A novel simplified equivalent modeling method for microstrip line interconnects. Indian Patent-202111019468. 2021.

[48] Belen MA, Mahouti P, Palandöken M. Design and realization of novel frequency selective surface loaded dielectric resonator antenna via 3D printing technology. Microwave and Optical Technology Letters. 2020; 62(5):2004-13.

[49] Patel DM, Raval F. Gain enhancement of SIW cavity-backed antenna using dielectric loading. Progress in Electromagnetics Research C. 2021; 111:61-73.

[50] Jing H, He G, Wang S. Design of a flexible cylindrical antenna with rotatable curved frequency selective surface for omnidirectional high-gain applications. International Journal of Antennas and Propagation. 2023; 2023:1-15.

[51] Ghosh A, Mandal T, Das S. Design of triple band slot-patch antenna with improved gain using triple band artificial magnetic conductor. Radioengineering. 2016; 25(3).

[52] Belabbas K, Khedrouche D, Hocini A. Artificial magnetic conductor-based millimeter wave microstrip patch antenna for gain enhancement. Journal of Telecommunications and Information Technology. 2021; 1(2021):56-63.

Shabnam Ara was born in U.P. India. She received B. Tech degree from G.E.I.T (H.N.B. University) in 2008 and her MTech degree from Graphic Era University in 2014. Currently, she is pursuing Ph.D at the University of Petroleum and Energy Studies, Dehradun. Since March 2019, she has been an Assistant Professor in the Electronics and Communication Engineering Department, at Shivalik College of Engineering in Dehradun. She has a total of 12 years of work experience including in industry and academics.
Email: shabnam.ara3012@gmail.com

Dr. Prasanthi Kumari Nunna was born in A.P., India. She received her B.Tech in Electronics and Communication Engineering from J.N.T.U. (Campus, Kakinada), an M.Tech in Digital Systems, Computer, and Electronics from J.N.T.U. (Campus, Ananthapur), and a Ph.D in Electronics from the University of Petroleum and Energy Studies, Dehradun, in 2015. Since 2009 she works as an Associate Professor at the University of Petroleum and Energy Studies in Dehradun. Her areas of expertise include low-power VLSI circuits, RF circuits, and metamaterials and their applications. She has a total of 20 years of experience.
Email: prasanti@ddn.upes.ac.in

Appendix I

S. No.	Abbreviation	Description
1	3G/4G/5G/5G	3rd Generation /4th Generation/5th Generation/6th Generation
2	ADS	Advanced Design System
3	AMC	Artificial Magnetic Conductor
4	ANN	Artificial Neural Network
5	C	Capacitor
6	CDMA	Code Division Multiple Access
7	CPW	Coplanar Waveguide
8	CSRR	Complementary Split Ring Resonator
9	DGS	Defective Ground Structure
10	DRA	Dielectric Resonator Antenna
11	EBG	Electromagnetic Band Gap
12	FBW	Fractional Bandwidth
13	FPC	Fabry-Perot Cavity
14	FPCA	Fabry-Perot Cavity Antenna
15	FBR	Front-to-Back-Ratio
16	FR4	Flame Retardant-4
17	FR1	Frequency Range (FR1)
18	FSS	Frequency Selective Surface
19	HFSS	High-Frequency Structure Simulator
20	ISM	Industrial Scientific and Medical
21	L	Inductor
22	LTE	Long Term Evolution
23	MMIC	Monolithic Microwave Integrated Circuits
24	MSE	Mean Square Error
25	R	Resistor
26	RLC	Resistor, Inductor, and Capacitor
27	PCB	Printed Circuit Board
28	RMSE	Root Mean Square Error
29	SIW	Substrate Integrated Waveguide
30	SMA	Subminiature Version A
31	SRR	Split Ring Resonator
32	SWB	Super-Wideband
33	VNA	Vector Network Analyzer
34	UWB	Ultra-Wide Band
35	VSWR	Voltage Standing Wave Ratio
36	UV	Ultra-Voilet
37	WB	Wideband
38	WLAN	Wireless Local Area Network